Modelling of FRP Confined Concrete under Uniaxial Compression Using CDPM2 in LS-DYNA

Thet Htar Nwe

MSc in Structural Engineering

ENG-5059P

Supervised by Dr. Peter Grassl

Abstract

In this project, FRP confined concrete model is developed using CDPM2 in LS-DYNA. Several finite element analyses are performed to predict the response of stress-strain relationship and to study the mechanic of confined concrete. Concrete is modelled as 4-node tetrahedron solid element and FRP is modelled as truss element in the analysis. The results of the proposed model were compared with the experimental results and the analytical results. The model was able to predict the response of FRP 1 layer confine concrete quite well. However, the model overestimated the ultimate strength of confined concrete for FRP 2 layers and 3 layers. The average error % increased with the number of FRP layers. In addition, the level of lateral expansion of concrete of the proposed model decreased with the number of FRP layers. Finally, the variation of concrete strength has the negative effect on the ultimate strength of confined concrete model.

Table of Contents

Preface

This project was carried out between June 2017 and August 2017 as part of the MSc. degree programme in Structural Engineering at University of Glasgow.

In this project, FRP confined concrete model was developed using CDPM2 in LS-DYNA. The verification of the model with the experimental results and the validation with the analytical results were included in the project.

I would like to express my sincere appreciation and thanks to my supervisor, Dr. Peter Grassl, for his constant guidance and valuable comments throughout this project.

List of Tables

List of Figures

1. Introduction

1.1 Background

Concrete has been the most well-known and versatile material due to its promising advantages such as high compressive strength, high durability and high temperature resistance. Although it has many advantages, strengthening or retrofitting of concrete structures is required as the degradation problems of concrete may arise from the exposure of harsh environment, seismic effects, corrosion of reinforcing steel, design inadequacy and poor workmanship (Giinaslan *et al*, 2014). High strength composites materials such as fibre reinforced polymers (FRPs) have been used to strengthen or retrofit in reinforced concrete structures due to its superior properties such as high corrosion resistance, high specific strength, high specific stiffness, high longitudinal tensile strength and ease of installation. Many researchers have proved that concrete strengthened with FRPs can improve strength and mechanical properties concrete structures.

The strengthening and retrofitting of concrete structures by using FRP confinement has been developed since 1990s (Benzarti & Colin, 2013). Many researchers have been investigating the behavior of FRP confined concrete by experimental results. And based on the experimental results, different stress-strain model for FRP confined concrete has been developed. However, due to the high cost of experiments, cost and time effective method is needed to investigate the stress-strain response of FRP confined concrete. Therefore, in recent years, many researchers are trying to propose models for FRP confined concrete using finite element analysis methods.

1.2 Aims and objectives of the project

The main objectives of the project are:

- to develop a finite element model for FRP confined concrete using CDPM2 in LS-DYNA,
- to verify the model by comparing the results from an experiment
- to validate the model by comparing the results from an analytical model, and
- to study the mechanics of concrete confined by FRP composite under uniaxial compressive loading,

1.3 Project outline

The first chapter is an introduction which provides the background and development of FRP composites in concrete structures. It also explains the objectives and outlines of the project. The second chapter is a literature review in which the background information of FRP composites, mechanics of FRP confined concrete, existing FE modelling approach and a material model CDPM2 have been reviewed. In addition, an experiment by Xiao and Wu (2000) and an analytical model by Youssef *et al* (2007), used to validate the developed model, are explained. In the third chapter, FE modelling approach, including material models, to develop the FRP confined concrete model are explained in detail. The fourth chapter includes the results and discussion in which the results from the FE model are compared with the experimental results and analytical results, and the mechanics of FRP confined concrete is analyzed. Conclusion and further research are in the last chapter, followed by a list of references and appendices.

2. Literature Review

2.1 Fibre Reinforced Polymer (FRP) Composites

2.1.1 Introduction

In recent years, many researches have been trying to investigate the effectiveness of fibre reinforced polymer (FRP) composites in strengthening reinforced concrete structures. It has been proved that FRP composites exhibit outstanding material properties such as high environmental resistance, high specific strength, high specific stiffness, high longitudinal tensile strength, low thermal and electric conductivity (Bhandari & Thapa, 2014; Singh, 2015).

There are two types of basic components in FRP composites: fibres and polymeric resin. Usually, continuous fibres such as carbon, glass and aramid fibres are embedded in a polymeric resin matrix material to form FRP composites. FRP composites can be found in the form of bars, sheets, strips and plates etc. The most common type of FRP is in the form of sheets (Bhandari & Thapa, 2014; Singh, 2015).Selection of fibre type and resin depend on the several factors such as required strength capacity, environmental resistance, and service life

2.1.2 Fibres and their properties

Fibres, in general, are long solid materials having a unique set of directional properties with high aspect ratio. When fibres are coated with polymeric film or other materials to protect surrounding environment, they become very durable and high strength material (Gowayed, 2013). Fibres can be in the form of continuous, woven or discontinuous fibres. In continuous form, fibres are normally long and straight fibres distributed parallel to each other. In woven form, fibres come in cloth form and provide multidirectional strength. In discontinuous form, fibres are generally short and randomly arranged (Giinaslan *et al*, 2014). Figure 2.1.2.1 shows the orientation of fibre in continuous, woven and discontinuous form.

Carbon, Glass and Aramid fibres are the most common types of fibres used in strengthening RC structures due to their superior properties such as light weight, high tensile strength and resistance to corrosion (Bhandari & Thapa, 2014; Piggott, 2004; Rashidi, 2014).

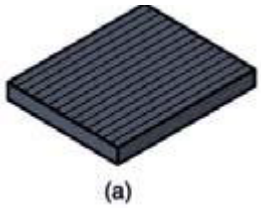

Figure 2.1.2.1: Fibre Orientation in (a) Continuous form, (b) Woven form, and (c) Discontinuous (Giinaslan et al, 2014)

Carbon fibres are brittle fibres which have excellent mechanical properties and thermal stability. They are two dimensional graphite sheets in a hexagonal layer network. They can be found in nature in forms such as diamond, graphite and ash. They can be made by pyrolysis of a hydrocarbon precursor. Carbon fibres available in the market are composed of three sources: Polyacrylonitrile (PAN), Pitch and Rayon (Gowayed, 2013, Singh, 2015). Typical mechanical properties of carbon fibres are shown in Table 2.1.2.1.

Table 2.1.2.1: Typical Mechanical Properties of Carbon Fibres (Hearle, 2001)

Precursor type	Product name	Tensile strength (MPa)	Young's modulus (GPa)	Strain to failure (%)
PAN	T300	3530	230	1.5
	T1000	7060	294	2.0
	M55J	3920	540	0.7
	IM7	5300	276	1.8
Pitch	KCF200	850	42	2.1
	Thornel P25	1400	140	1.0
	Thornel P75	2000	500	0.4
	Thornel P120	2200	820	0.2

Glass fibres have been the most widely used fibre in civil engineering application due to high specific strength, high temperature resistance and low cost (Murali & Pannirselvam, 2011; Singh, 2015). Glass fibres are silica-based glass compounds. They are available in industry in the form of roving, woven roving, chopped stand mats, uni-directional cloth (Ramamoorthy & Tamilamuthan, 2015; Singh, 2015). Glass fibres typically used in FRP composites can be classified into E-glass (for electrical), S-glass (for strength) and C-glass (for corrosion) (Gowayed, 2013). E-glass fibres are electrical insulators; they are most widely used type which comprises approximately about 80%-90% of the glass fibre industry. S-glass fibres exhibit higher strength and higher temperature performance than E-glass; they are the most expensive type and manufacture under specific quality control. C-glass fibres are highly resistance to corrosion; they have chemical stability in corrosive environments (Singh, 2015). Typical Mechanical properties of different type of glass fibres are shown in Table 2.1.2.2.

Table 2.1.2.2: Typical Mechanical Properties of Different Types of Glass Fibres (Gowayed, 2013)

	Tensile strength (MPa)	Tensile modulus (GPa)	Poisson's ratio	Density (g/cm^3)	Strain to failure (%)
E-glass	3450	3.45	0.22	2.55	1.8-3.2
C-glass	3300	69	-	2.49	-
S-glass	3500	87	0.23	2.5	4

Aramid fibres are organic fibres and are very rigid and rod-like materials which belong to liquid crystal polymers. They are available in the form of tows, yarns, rovings and woven cloths (Singh, 2015). Aramid fibres exhibit high thermal stability, high strength and high modulus. They are anisotropic material; they have higher tensile strength in fibre direction and lower strength in other directions. Under compression and bending, aramid fibres exhibit lower strength, and therefore, are not suitable for shell structures unless hybridized with glass or carbon fibres to carry high compressive and bending loads (Singh, 2015). Typical properties of aramid fibres are shown in Table 2.1.2.3.

Table 2.1.2.3: Typical Properties of Aramid Fibres (Singh, 2015)

Type of Aramid Fibres	Tensile strength (MPa)	Tensile modulus (GPa)	Poisson's ratio	Density (g/cm^3)	Strain to failure (%)
Kevlar 49	3620	131	0.35	1.44	2.8
Twaron 1055	3600	127	0.35	1.45	2.5

2.1.3 Polymer resins and their properties

The polymeric resin matrix acts as the glue that allows the fibers to work as a single filament. When the load is applied, the matrices deform and transfer the stresses to the fibres which have higher modulus. The function of the matrix is to hold the fibre together, transfer the stress between the fibres and the adjacent structural elements, and helps in protecting fibres form environmental and mechanical damage. Although fibres themselves are susceptible to moisture attack, due to the resistance of moisture attack by the resin matrix, the corrosion of the composite material become minimum (Giinaslan *et al*, 2014; Shao, 2003; Singh, 2015).

The polymeric matrices are either thermosetting or thermoplastic. Thermoset matrices are resins that are formed by cross-linking polymer chains; they cannot be melted or recycled because the polymer chains form a three-directional network. The continuous fibres are usually stiffer and stronger than the matrix in thermosetting matrices. Examples of thermosetting matrices used in FRPs are epoxy, polyester, phenolic and vinylester. Unlike thermoset matrices, thermoplastic matrices are not cross linked; but they can be remelted and recycled. Examples of thermoplastic matrices used in FRPs are nylon, polyethylene and terephalate (Singh, 2015). Epoxy and polyesters are the most common types of resin used in strengthening RC structures due to having good adhesion characteristics, high toughness, good curing property and providing stability to the fibres (Bhandari & Thapa, 2014). It is important to carefully choose the types of resin which has higher maximum strain limit, especially applied in large structures, to obtain the optimal performance

(Singh, 2015). Table 2.1.3.1 shows the mechanical properties of typical resin used in FRP composites.

Table 2.1.3.1: Typical Mechanical Properties of Resins (Hollaway,1990)

	Polyester Resin	Epoxy Resin
Density (g/cm^3)	1.20-1.4	1.1-1.35
Tensile Strength (MPa)	44.82-90.32	40-100
Compressive Strength (MPa)	100-250.28	100-200
Tensile Modulus of Elasticity (GPa)	2.5-4	3-5.5
Poisson's Ratio	0.37-0.4	0.38-0.4
Coefficient of Thermal Expansion ($10^{-}0/^{o}C$)	100-120	45-65
Shrinkage at Curing (%)	5-8	1-2

2.1.4 FRP composites and their properties

FRP composites are usually anisotropic material, i.e. different properties in different directions. If the fibres are oriented only in one direction, the FRPs are said to be unidirectional composite. If the fibres are oriented in perpendicular to each other, then the properties of FRPs in these directions are superior to the properties in other directions depending on the volume of fibres provided. Only in the direction of fibres, tensile strength is high. Anisotropic fibres in FRPs provide optimal strength and modulus in the direction of the fibre axis. Due to the property of anisotrophe, the optimum design can be obtained by providing the material only in the required direction which leads to inexpensive solution to critical loading scenario (Gowayed, 2013; Singh, 2013).

FRP composites exhibit material properties such as high specific strength, high specific stiffness, high environmental resistance, and low thermal and electric conductivity (Singh, 2015; Bhandari & Thapa, 2014). Table 2.1.4.1 shows typical properties of concrete, steel and FP composites. The most important factors affecting the mechanical properties of FRP composites are: fibre orientation, length, shape, compositions of fibres and resin matrix, the adhesion of bond between fibres and the matrix, volume fraction of fibres in the overall mix, and fabrication technique (Piggot, 2004; Shao, 2003; Singh, 2015).

Table 2.4.1: Typical Properties of Concrete, Steel and FRP Composites (Habib, 2017; Piggott, 2004)

Reinforcing Material	Yield strength (MPa)	Tensile Strength (MPa)	Modulus of Elasticity (GPa)	Compressive Strength (MPa)	Strain at Failure (%)
Concrete	N/A	1.6-5.0	27-44	12-90	N/A
Steel	276-517	280-1900	190-210	N/A	N/A
Carbon FRP	N/A	1720-3690	120-580	N/A	0.5-1.9
Glass FRP	N/A	480-1600	35-51	N/A	1.2-3.1
Aramid FRP	N/A	1035-1650	45-59	N/A	1.6-3.0

Note:

- It is understood that steel has an ultimate tensile strength, however, it is not used in design.
- The values given for the various FRPs are based on a typical fiber volume fraction of 0.5 to 0.7.
- ACI 440.6-08 specifies that glass fiber and carbon fiber based reinforcing bars have a tensile elastic modulus of at least 5,700 ksi (39.3 GPa) and 18,000 ksi (124 GPA), respectively.

Although FRPs have many advantages, they have some weaknesses that entail particular attention when used as structural materials. Unlike steel, FRPs materials are very brittle and do not show yielding before brittle rupture; they have low transverse strength and low modulus of elasticity (Singh, 2015). The stress-strain relationship for fiber, resin matrix and composite material is shown in figure 2.1.4.1. Fibre and composite generally exhibit linear elastic behaviour, while resin matrix are visco-elastic or visco-plastic (Shao, 2003).

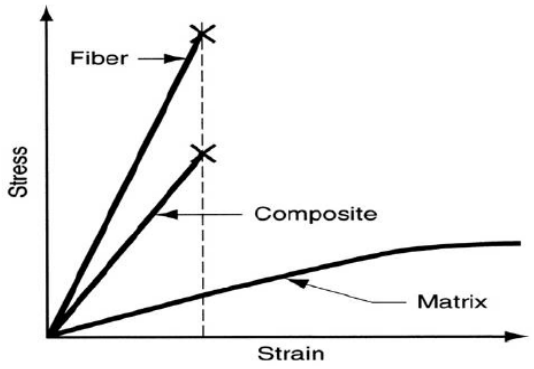

Figure 2.1.4.1: Stress-Strain Diagram for Composite Phases (Giinaslan et al, 2014)

2.2 Mechanics of FRP confined concrete

The concrete structures are susceptible to unusual loading such as seismic loads and impact explosion. When subjected to these loadings, concrete structures are required to repair or retrofit to maintain the desired load capacity or increase the performance of concrete such as strength and ductility. This can be done by wrapping concrete externally with FRP sheets to provide confining action to the concrete (Ramamoorthy & Tamilamuthan, 2015; Youssef *et al*, 2007). When the concrete is externally wrapped with FRP laminates, the fibres in the hoop direction resist the traverse expansion of the concrete. The pressure that resists the lateral expansion is called the confining pressure (Bhandari & Thapa, 2014). The lateral confining pressure in FRP confined concrete increases continuously with loading (Pan *et al*, 2017). In confining circular columns, the FRP jackets produce the uniform confining pressure around the parameter of the circular column as shown in figure 2.2.1. However, in confining square or rectangular columns, FRP jackets produce the confining pressure stress concentrated around the edges of such columns and the failure takes place at one of the corners due to the rupture of FRP jackets (Youssef *et al*, 2007). Figure 2.2.2 shows the confinement of concrete rectangular/square columns with FRP composite jackets.

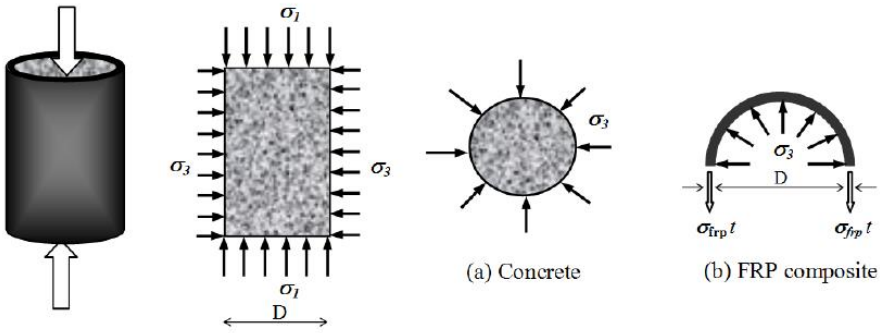

Figure 2.2.1: Scheme of Confining Action for (a) Concrete, (b) FRP composite (Girgin, 2014)

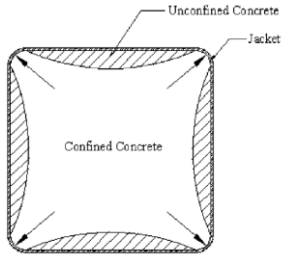

Figure 2.2.2: Confinement of Concrete Rectangular/Square Columns with FRP Composite Jackets (Youssef et al, 2007)

Under uniaxial compressive loading, the concrete tends to expand laterally due to Poisson's effect (Bhandari & Thapa, 2014). When the lateral expansion of concrete is confined by FRP layers, the stress state of concrete converts into triaxial compressive stress state. This triaxial compressive stress helps to provide better performance in terms of strength and ductility compared to concrete under normal uniaxial compression (Bhandari & Thapa, 2014; Ramamoorthy & Tamilamuthan, 2015; Rashidi, 2014).

In FRP confined concrete, the stress-strain curve is characterized by a distinct bilinear response with a transition zone at a stress level near the strength of unconfined concrete (Ramamoorthy & Tamilamuthan, 2015). At low level of axial stress, concrete behaves elastically. At this stage, the axial strain is low and the transverse strain is relatively proportional to the axial strain by the Poisson's ratio. As the transverse strain is also low, FRP jackets induce low confining pressure. As the load increases, the dilation of concrete due to the formation of cracks starts to occur resulting in the noticeable increase of transverse tensile strain, and the effect of FRP laminates become more significant (Bhandari & Thapa, 2014; Youssef *et al*, 2007). The stress-strain relationship of CFRP confined concrete with 0 layer, 1 layer, 2 layers and 3 layers is shown in figure 2.2.3.

There are two important factors affecting the concrete confinement. The first factor is the tendency of concrete to dilate after cracking, and the other factor is the radial stiffness of FRP wrapping to restrain the concrete dilation (Bhandari & Thapa, 2014; Youssef, 2007).

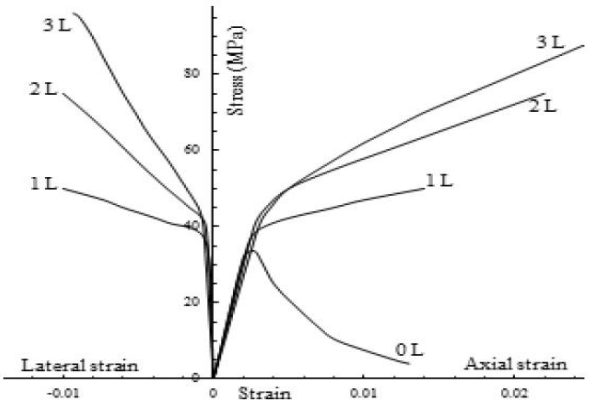

Figure 2.2.3: Stress-strain Relationships for FRP Confined Concrete (Xiao & Wu, 2000)

2.3 Background of FE modelling of FRP confined concrete

Reinforced concrete structures are usually design to satisfy the serviceability and safety requirement of concrete. The prediction of cracking and deflection are needed to consider ensuring the serviceability design requirement of the concrete structures. In terms of safety, the estimation of maximum limit of loading capacity is required to be taken into consideration. Therefore, load-deflection, stress-strain relations, cracked pattern and deformed shape of concrete structure are the important criteria in predicting the characteristics of the concrete structures (Ramamoorthy & Tamilamuthan, 2015). It has been proved by many experimental results that the strengthening of concrete using FRP sheets enhance the structural behavior of concrete. Recently, researchers are trying to understand the confinement mechanism and introduce suitable models for the behavior of confined concrete in RC structural concrete. Fardis and Khalili (1982) made the first attempt at developing a confinement model for FRP-wrapped concrete. Over the years, a large number of confinement models have been developed for concrete columns. These models can generally be classified into two categories: design-oriented model and analysis-oriented model (Pan *et al,* 2017).

Design-oriented models are models in closed-form expression, i.e. by using the equations and are directly based on the interpretation of experimental results. In analysis-oriented model, the stress-strain curve of the FRP confined concrete can be generated through an incremental process under different level of active confinement. The accuracy of analysis-oriented models depends on the accuracy of the lateral-to-strain relationship and failure

surface defined for the actively confined concrete. In general, the design of RC is based on the rational analytical procedures. However, due to the inaccuracy and complexity of the analytical method, many design methods are still relying on the data obtained from a large number of experimental results. Again, it is relatively costly to carry out the experiments. Recent years, cost and time effective method of analyzing the behavior of concrete structures by using finite element (FE) analysis software has developed and widely used. To validate the finite element model, the results from finite element analysis are compared with the results obtained from the experimental tests. The experimental results are still carrying out since a frim basis for design equations can be provide and the validation of finite element models can be done from the experimental results (Ramamoorthy & Tamilamuthan, 2015, Pan et al, 2017).

In the finite element modelling, the properties of constituent materials, geometric nonlinearities of the concrete structures, complexity of the model, understanding of the software used, and advanced meshing method for nonlinear analysis of the structure are taken into consideration. To set up the model, these parameters should be investigated first to achieve the optimum prediction of the behaviour of the structure. If the model is complex and lack of symmetry, it is better to create the whole model instead of modelling parts to obtain the most precise result as a representative of the true specimens. However, modelling and analysing the whole model require relatively massive amount of time (Rashidi, 2014). Therefore, it is sometimes possible to model only parts of the structure instead of modelling the whole structure to improve the calculation speed of analysis. In such cases, the symmetry constraints are applied in the symmetry planes (Pan *et al*, 2017).

In finite element modelling of FRP confined concrete columns, it is usually modelled with separate elements and combined it to act as the whole strucutres. FRP condined concrete can be divided into two main elements in general: concrete and FRP composites.

For concrete, it can be modelled by two options: elastic nonlinear option and elastic-plastic nonlinear option. Elastic nonlinear option depends in stress-strain curve and maximum stress yield criterion; whereas, elastic-plastic nonlinear option depends on the Drucker-Prager yield criterion. The first option does not consider the effect of lateral expansion of the concrete. The second option, which is based on elastic-plastic nonlinear behaviour, is preferable as it is capable of exhibiting the effect of confining concrete

structure (Rashidi, 2014). Typically, solid elements are used to model concrete columns (Pan *et al*, 2017; Ramamoorthy & Tamilamuthan, 2015). These solid elements have three degrees of freedom at each node – translations in the nodal x, y, and z directions. The elements are capable of plastic deformation, cracking in three orthogonal directions, and crushing. The geometry of 8-node solid element is shown in figure 2.3.1. FRP composite is usually modelled as a layered solid element. The layered solid element allows for up to 100 different material layers with different orientations and orthotropic material properties in each layer. The element has three degrees of freedom at each node and translations in the nodal x, y, and z directions. The geometry, node locations and the coordinate system of a layered solid element is shown in figure 2.3.2. However, Pan *et al* (2017) used shell element with Drucker Prager yield criterion to simulate FRP composites in confined concrete.

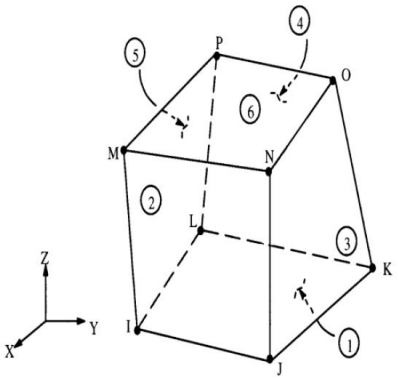

Figure 2.3.1: 8-Node Solid Element Geometry and Nodes Location (Ramamoorthy & Tamilamuthan, 2015)

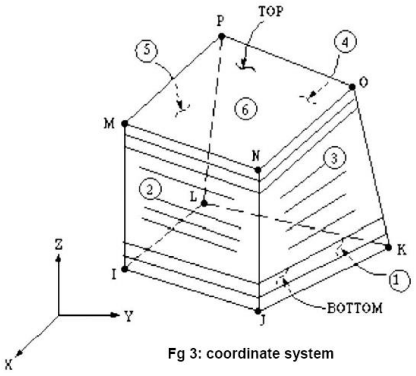

Figure 2.3.2: Geometry, Node Locations and Coordinate System (Ramamoorthy & Tamilamuthan, 2015)

Previous finite element analysis with refined meshes are performed with commercially available software such as STRAND7, ANSYS and ABAQUS. Due to massive amount of elements and degrees of freedom included in the models to analyse structural behaviour in these software, the computational cost is extremely expensive (Hu & Barbato, 2014). Therefore, the advanced modelling approach to analyse 3D nonlinear response of the structures is required to develop. Desprez *et al* (2013) and Hu and Barbato (2014) modelled FRP confined concrete columns by using advanced nonlinear constitutive modelling strategy. In their strategy, mulitfibre Timoshenko beam (Desprez et al, 2013) or Euler-Bernoulli beam (Hu & Barbato, 2014) element are used for spatial discretization, and introduced in the finite element code FEDEASLab (a MATLABtoolbox) in order to simulate nonlinear behaviour at fibre level. In FEDEASLab, a number of options for load and time steeping scheme and iterative schemes can be selected to analyse nonlinear static and dynamic behaviour of structures (Hu & Barbato, 2014). Figure 2.3.3 shows multifibre discretization of confined concrete.

Figure 2.3.3: Multifibre Discretization (Desprez, et al, 2013)

The reinforced confined concrete column is simulated by using numerous beam elements with cross sections divided into fibers. A constitutive model is corrrelated with each fiber. This model allows to decrease the number of degree of freedom resulting a useful tool for earthquake engineering. In addition, this model simplifies the finite-element mesh and reduces the computation cost of analysis.

As many researchers gained a lot of interest in retrofitting, further research has focused on the external confinement models related to steel and FRP wraps. In order to develop efficacious predictive tools for seismic retrofitting of RC structures, it is required to correctly simulate the cyclic behaviours of internally confined transverse steel reinforcement and externally confined FRP. Although various models have been developed for cyclic loading with plain concrete and steel-confined concrete, according to (Desprez *et al*, 2013), it is found that only two models have been proposed for cyclic loading and FRP. Moreover, they only deal with compression, and are not able to consider FRP confinement. Therefore, the applicability of stress-strain model for confined concrete is limited.

2.4 Concrete Damage Plasticity Model 2 (CDPM2)

Many constitutive models to predict nonlinear response of concrete have been developed in the previous literature. These models are based on the theory of plasticity, damage mechanics and combination of plasticity and damage mechanics (Grassl *et al*, 2013). In this chapter, the background theory of the constitutive model for concrete used in this project will be discussed.

Grassl *et al* (2013) states that stress-based plasticity models are capable of describing the observed deformation in modelling confined compression, however, they cannot present the behaviour of stiffness reduction in unloading process. On the other hand, strain-based damage mechanics models are useful for modelling concrete to describe the stiffness degradation in tensile and low confined compression, and yet, they are not able to describe the observed irreversible deformations. In order to obtain a better constitutive model for modelling both tensile and compressive failure, the combination of stress-based plasticity model and strain-based damage mechanic model has been well developed and widely used. These combined models are called damage-plastic models.

One of the well-known damage-plastic models developed by Grassl and Jirasek (2006) is called Concrete Damage Plasticity Model 1 (CDPM1). CDPM1 works well with concrete subjected to multiaxial stress states. This model depends on the single damage variable in both tension and compression. It is capable of describing the characteristics of monotonic

loading with unloading, but not suitable for describing the transition from tensile to compression failure.

CDPM2 is a modified version of CDPM1. There were three improvements in CDPM2 compared to CDPM1. These three improvements were as follows: (1) hardening was introduced in the post-peak regime of the plasticity part of the model, (2) two damage variables were introduced for tension and compression separately, and (3) strain rate dependence was introduced in the damage function. This model is capable of describing the effects of confinement on strength, observed deformation, irreversible displacements and the degradation of stiffness, and also the transition from tensile to compression failure realistically. In addition, CDPM2 is also capable of describing concrete failure mesh independently (Grassl *et al*, 2013).

The damage plasticity model depends basically on the following stress-strain relationship:

$$\sigma = (1 - \omega_t)\bar{\sigma}_t + (1 - \omega_c)\,\bar{\sigma}_c \qquad (2.4.1)$$

where, σ is the stress for damage plasticity model, ω_t and ω_c are two scalar damage parameters, ranging from 0 (undamaged) to 1 (fully damaged), and $\bar{\sigma}_t$ and $\bar{\sigma}_c$ are the positive and negative parts of the effective stress tensor $\bar{\sigma}$.

The effective stress tensor $\bar{\sigma}$ is defined according to the damage mechanics convention as:

$$\bar{\sigma} = D_e : (\varepsilon - \varepsilon_p) \qquad (2.4.2)$$

where, D_e is the elastic stiffness tensor, ε is the strain tensor and ε_p is the plastic strain tensor.

Plasticity:

The plasticity part of the model is formulated in a three-dimensional framework with a pressure-sensitive yield surface, non-associated flow rule and hardening laws. The yield surface is described by the Haigh-Westergaard coordinates: the volumetric effective stress, the norm of the deviatoric effective stress and the Lode angle. The flow rule is non-associated as the associated flow rule would produce an overestimated maximum stress for concrete (Grassl, 2016). The hardening laws influence the shape of the yield surface. The main equations for plasticity model are:

$$f_p(\bar{\sigma}, \kappa_p) = F(\bar{\sigma}, q_{h1}, q_{h2}) \quad (2.4.3)$$

$$\dot{\varepsilon}_p = \dot{\lambda} \frac{\partial g_p}{\partial \bar{\sigma}} (\bar{\sigma}, \kappa_p) \quad (2.4.4)$$

$$f_p \leq 0, \ \dot{\lambda} \geq 0, \ \dot{\lambda} f_p = 0 \quad (2.4.5)$$

where, f_p is the yield function, κ_p is the plastic hardening variable, q_{h1} and q_{h2} are dimensionless functions controlling the evolution of the size and shape of the yield surface, $\dot{\varepsilon}_p$ is the rate of the plastic strain, $\dot{\lambda}$ is the rate of plastic multiplier and g_p is the plastic potential which is controlled by the hardening law. Superimposed dot indicated the derivative with respect to time, but the model is as the rate-independent and the rate is considered as infinitesimal increments (Grassl *et al*, 2013).

Damage:

The damage part of the model can be described by the damage loading functions, the evolution law for the damage variables and the loading-unloading conditions for tension and compression (Grassl *et al*, 2013). The main equations for damage model are:

$$f_{di} = \alpha_i \tilde{\varepsilon}_i(\bar{\sigma}) - \kappa_{di} \quad (2.4.6)$$

$$f_{di} \leq 0, \ \dot{\kappa}_{di} \geq 0, \ \dot{\kappa}_{di} f_{di} = 0 \quad (2.4.7)$$

$$\omega_i = g_{di}(\kappa_{di}, \kappa_{di1}, \kappa_{di2}) \quad (2.4.8)$$

where, index ‘i’ refers to ‘t’ for tension and ‘c’ compression, f_{di} is the loading function, α_i is a variable that distinguished between tensile and compression loading, $\tilde{\varepsilon}_i$ is the equivalent loading, and $\kappa_{di}, \kappa_{di1}, \kappa_{di2}$ are the damage variables.

A detailed description of CDPM2 is given in Grassl *et al* (2013).

.

2.5 Experiment for Comparative Study

Verification of FE modelling is usually made by comparing the response of FE models with the experimental results. This chapter will present the experiment performed by Xiao and Wu (2000) which will be compared with the results from FE model by LS-DYNA proposed in this project.

2.5.1 Specimen

A total of 36 concrete cylinders with a height of 305 mm and a diameter of 152 mm were tested in the experiment. The varying parameters of the experiment were concrete strength and thickness of CFRPs. The compressive strengths of concrete at 28 days were 27.6 MPa, 37.9 MPa and 48.2 MPa for lower strength, medium strength and high strength respectively. Concrete strengths were a bit higher than the target strength at the time of testing. The actual concrete strength at the time of testing were 33.7MPa, 43.8MPa, and 55.2MPa.

For each batch of concrete, 12 cylinder specimens were cast under standard procedure and cured in a close-can at normal room temperature. From each concrete batch, 3 concrete specimens were tested without FRP confinement, 3 specimens with 1 layer of FRP confinement, 3 specimens with 2 layers of FRP confinement and 3 specimens with 3 layers of FRP confinement. Table 2.5.1.1 summarizes the test matrix.

Table 2.5.1.1: Test Matrix (Xiao & Wu, 2000)

Type of jacket	Concrete strength	Jacket layers	Specimen numbers
Carbon fibre sheet reinforced composite jacket	Lower	Plain concrete 1-layer 2-layer 3-layer	3 specimens 3 specimens 3 specimens 3 specimens
	Medium	Plain concrete 1-layer 2-layer 3-layer	3 specimens 3 specimens 3 specimens 3 specimens
	Higher	Plain concrete 1-layer 2-layer 3-layer	3 specimens 3 specimens 3 specimens 3 specimens

The FRP jackets were applied directly to the surfaces of concrete cylinders, which were pre-treated with primer epoxy, providing unidirectional lateral confinement in the circumferential direction of the concrete cylinder. In order to obtain the full enhancement of composite tensile strength, an overlap of 152mm was used to wrap the cylinder. The mechanical properties of the CFRP sheets were obtained from the Tension Coupon Tests following the ASTM Specification D 3039-75 (Standards 1990). Table 5.1.2 presents the averaged mechanical properties of CFRP composites used in the experiment:

Table 5.1.2: Mechanical properties of CFRP composite (Xiao & Wu, 2000)

System	Thickness per ply (mm)	Young's modulus, Ej (MPa)	Tensile strength, f_{ju} (MPa)	Failure strain, ε_{ju} (%)
Carbon/epoxy	0.381	1.05×10^5	1,577	1.5

2.5.2 Test Setup

The experiment was performed using a special compression testing machine at the Structural Laboratory of the University of the Southern California. The machine was equipped with a high-tech computerized control and data acquisition system. Figure 2.5.2.1 illustrates the testing and instrumentation configurations.

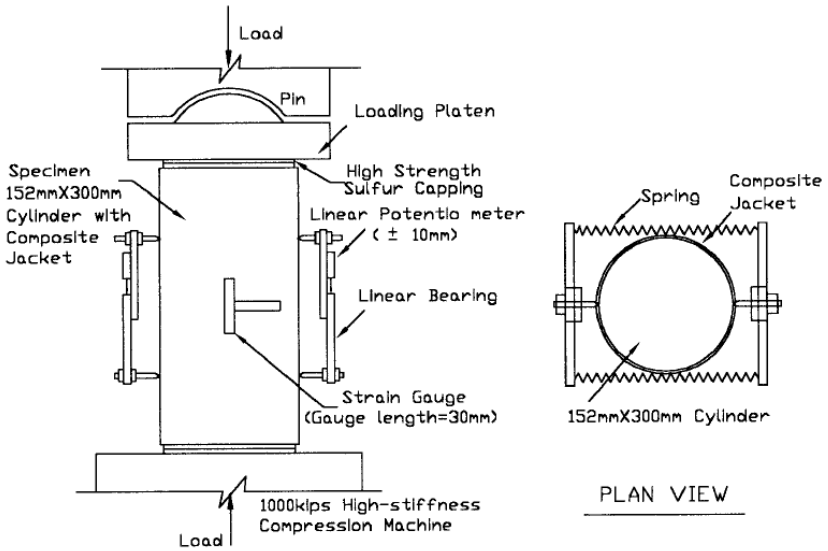

Figure 2.5.2.1: Test and Instrumentation Configurations (Xiao & Wu, 2000)

The applied load, axial deformation of concrete and axial and transverse strains of FRP jackets were obtained from the machine. The axial deformation of the concrete was measured in the middle portion with an advanced device containing a linear potentiometer and a linear bearing. The strains of the FRP jackets were measured with strain gauge which was placed at mid height of the specimen. Both ends of the concrete cylinders were capped with high-strength Sulphur in order to distribute the loads uniformly, resulting in reduction of load eccentricity.

In the test, all the specimens failed by the rupture of the FRP jacket.

2.6 Analytical model for FRP Confined Concrete

Validation of FE modelling in this project is made by comparing the stress-strain behavior of confined concrete with the analytical model by Youssef *et al* (2007). This chapter discusses the theory of the analytical model by Youssef et al (2007).

Youssef *et al* (2007) proposed an analytical model to theoretically predict the behavior of FRP confined concrete. Their model was based on the experimental data conducted in their study. During the experiment, the stress-strain response of the tested specimens exhibited three different stages during the experiment:

Stage-1 indicated that the early phase of the stress-strain behavior of FRP confined concrete traced the path of unconfined concrete, and therefore, the initial path of the stress-strain curve for confined concrete was considered as the confined modulus of elasticity E_c. In Stage-2, when the strength of unconfined concrete was exceeded, the stress-strain curve became soften until it reached the point where FRP confining action was fully activated. In Stage-3, the FRP jacket was fully activated and the confining stress of FRP jackets increased proportionately to the applied load showing linear response up until the rupture of the jacket.

The general stress-strain curve for FRP confined concrete based on these stages is shown in figure 2.6.1. *Point-A* represents the origin of the stress-strain curve where the axial stress and axial strain is zero. *Point-B* represents the end of Stage-2 where FPR jacket is fully activated. And *Point-C* represents the ultimate condition where the ultimate strength of FRP jacket is reached.

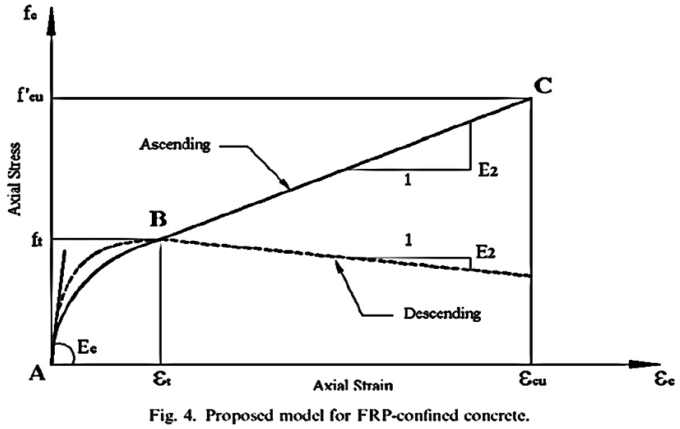

Fig. 4. Proposed model for FRP-confined concrete.

Figure 2.6.1: Proposed model for FRP confined concrete (Youssef et al, 2007)

In order to describe the analytical stress-strain curve of FRP confined concrete, several parameters were determined. These parameters were the confined modulus of elasticity E_c, axial stress f_t, axial strain ε_t, ultimate stress of FRP-confined concrete f'_{cu} and ultimate concrete compressive strain ε_{cu}.

The equations for these parameters are:

$$E_c = 4700\sqrt{f'_c} \tag{2.6.1}$$

$$f_t = \left\{1.0 + 3.0\left(\frac{\rho_j E_j \varepsilon_{jt}}{f'_c}\right)^{5/4}\right\} f'_c \tag{2.6.2}$$

$$\varepsilon_t = 0.002 + 0.0775\left(\frac{\rho_j E_j \varepsilon_{jt}}{f'_c}\right)^{6/7}\left(\frac{f_{ju}}{Ej}\right)^{1/2} \tag{2.6.3}$$

$$f'_{cu} = \left\{1.0 + 2.25\left(\frac{f'_{lu}}{f'_c}\right)^{5/4}\right\} f'_c \tag{2.6.4}$$

$$\varepsilon_{cu} = 0.003368 + 0.2590\left(\frac{f'_{lu}}{f'_c}\right)\left(\frac{f_{ju}}{Ej}\right)^{1/2} \tag{2.6.5}$$

where, f'_c is the compressive strength of unconfined concrete, ρ_j is the confinement ratio, E_j is the tensile modulus of FRP jacket, ε_{jt} is the FRP jacket strain at transition from first

to second region, f_{ju} is the tensile strength of FRP jacket, and f'_{lu} is the effective lateral confining stress at ultimate condition of the FRP jacket.

A detailed description for this stress-strain model can be found in Youssef *et al* (2007).

3. FE Modelling Approach in LS-DYNA

3.1 General

In this project, finite element modelling to predict the response of FRP confined concrete was carried out in general purpose FE program called LS-DYNA. LS-DYNA is capable of simulating complex real world problem, and therefore, it is used in the construction, manufacturing, bioengineering, automobile and aerospace industries. LS-DYNA contains a single executable file and is driven entirely by command line. Therefore, only a command shell, the executable and the input files are required to run LS-DYNA. In addition, all the input files are ASCII (American Standard Code for Information Interchange) format, and therefore, the input files can be prepared with input cards in any text editor or with the instant aid of a graphical processor. The pre-processing of LS-DYNA can be performed in the third party software called LS-PrePost or LS-OPT (LSTC, 2011).

In this project, the input files for FE modelling of CFRP confined concrete were prepared using the text editor. There were three main input files, referred to as 'keyword' or '.k' file namely: 'input.k', 'mesh.k', and 'material.k'. All the information about time step, analysis controls, output parameters, and the command to run 'mesh.k' and 'material.k' files are included in the 'input.k' file. All the information about nodes, elements, set of nodes and elements, and the boundary conditions are included in 'mesh.k' file. And the 'material.k' file includes the information about the material model used in this project. The advantage of having three separate files is that when modifying the 'mesh,k' file, the input and material information in other two files will not be overwritten. The input files for this project are presented in Appendix Section.

3.2 Model Geometry

The concrete core of the cylinder, with a diameter of 152 mm and a height of 305 mm, was modelled using 4-node tetrahedron solid element as this element is suitable for material with high compressibility. Truss element was used to model the CFRP jacket as this element is implemented for elastic and elastic-plastic material with kinematic hardening and it carries axial force only. It has three degrees of freedom at each node

(LSTC, 2017). Figure 3.2.1 illustrates 4-node tetrahedron solid element and figure 3.2.2 illustrates truss element.

The trusses were fully installed around the perimeter of the concrete core to obtain the confinement action of FRP jackets. For the truss element, only the cross-sectional area was required to be defined in LS-DYNA input card. Therefore, the total area of the FRP jacket was given the same as the total area of trusses.

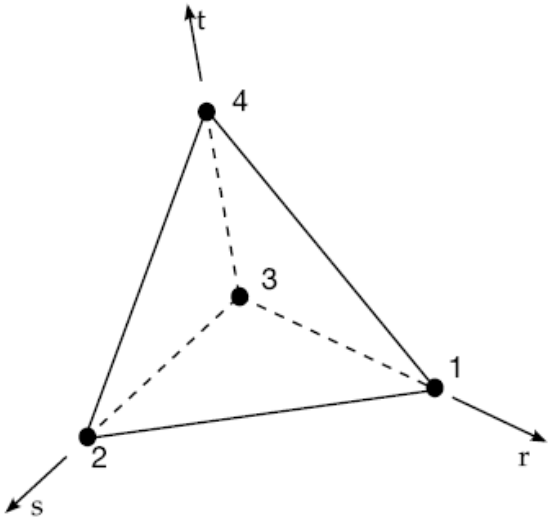

Figure 3.2.1: 4-Node Tetrahedron Solid Element (LSTC, 2017)

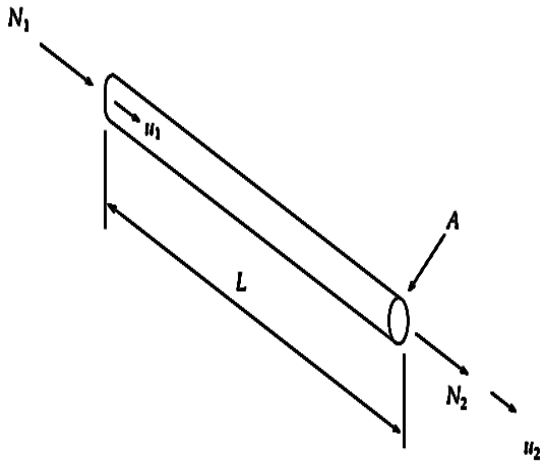

Figure 3.2.2: Truss Element (LSTC, 2017)

The concrete core and FRP jackets were assumed to have a perfect bond. Therefore, the same nodes were sharing at the contact surface of the tetrahedron element and truss element. In order to create uniform tetrahedral meshes for concrete core, T3D Mesh

Generator, a very good mesh generator for tetrahedron element provided by Daniel Rypl (2004), was used. Figure 3.2.3 shows the finite element mesh for FRP confined concrete model for mesh size of 0.05 m.

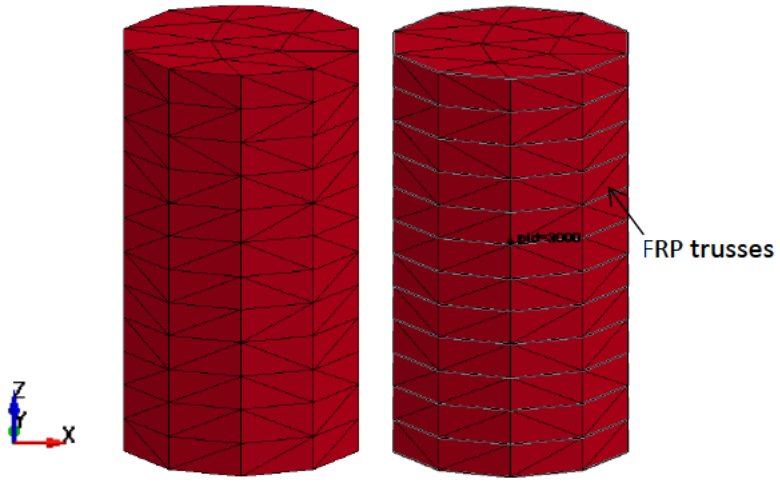

Figure 3.2.3: Finite Element Mesh for FRP Confined Conrete Model (mesh size = 0.05m)

3.3 Boundary and Loading Condition

The concrete model was subjected to uniaxial compression in Z-direction. This compression loading was uniformly applied to every nodes on the upper surface of the concrete core. Therefore, the nodes on the upper surface were linked as a node set using BOUNDARY_PRESCRIBED_MOTION card in 'mesh.k' file, and the displacement was prescribed in the card. In addition, all nodes from the lower surface of the concrete core were connected using BOUNDARY_SPC card. The node set for the lower surface of the concrete core was restrained in Z-direction, but the node set for the surface of the concrete core was set to move freely in Z-direction as the displacement was applied in the upper node set. One of the nodes from the upper surface and one from the lower surface were fixed in both X and Y-direction to prevent the concrete core from moving. No rotational restraints were applied.

3.4 Material Models

The concrete core was modelled using Concrete Damage Plasticity Model 2 (CDPM2) by (Grassl *et al*, 2013) and FRP was modelled as elastic material in this project. The

information for CDPM2 was inserted in the input card entitled as '*MAT_CONCRETE _DAMAGE_ PLASTIC _ MODEL' (*MAT_CDPM). Likewise, the information for elastic material was inserted in the input card called '*MAT_ELASTIC or MAT_001'. The input cards were included in the 'material.k' file.

3.4.1 Material Model for Concrete (*MAT_CDPM)

The material model used for the concrete core was the '*MAT_CONCRETE_ DAMAGE_PLASTIC_MODEL' (*MAT_CDPM) by Grassl (2016). This model is an extended description of MAT_273 input. This model is based on effective stress plasticity and with a damage model based on both plastic and elastic strain measures. This model works only for solid elements. There are 24 input variables in the input card in LS-DYNA. Most of the variables have default values that are based on experimental data. However, the default values are not suitable for all types of concrete or load path. Therefore, a number of variables were needed to be determined in compliance with this project. Only the modified variables will be explained in this section.

The modified variables were mass density (RHO), Young's modulus (E), Poisson's ratio (PR), uniaxial tensile strength (FT), uniaxial compressive strength (FC), hardening parameter (HP), tensile damage type (TYPE), tensile threshold value for linear tensile damage formulation (WF), parameter controlling compressive damage softening branch in the exponential compressive damage formulation (EFC).

- Mass density of concrete (RHO) was taken as 2300 kg/m^3 for all analyses in this project since CEB-FIP Model Code (2010) provides the normal weight of concrete as 2000-2600 kg/m^3 for normal weight concrete.
- Young's modulus of concrete (E) was calculated according to CEB-FIP model code (2010) by using the equation:

$$E = E_{co} \cdot \alpha_E \cdot \left(\frac{f_{cm}}{10}\right)^{1/3} \qquad (3.4.1.1)$$

where, E_{co} is taken as 21.5 x 10^3 MPa, α_E is 1 for quartzite aggregates, and f_{cm} is the actual compressive strength of concrete at an age of 28 days. The values used in this project were 30.16x10^3 MPa, 33.52x10^3 MPa and 36.32x10^3 MPa for low strength, medium strength and high strength concrete respectively.

- Poisson's ratio (PR) was taken as 0.2 for all analyses in this project as Bright and Roberts (2010) gives Poisson's ratio of 0.2 for all uncracked concrete.

- Uniaxial tensile strength (FT) was calculated according to the CEB-FIP Model Code (2010) by using the equation:

$$FT = 0.3\ (f_{ck})^{2/3} \tag{3.4.1.2}$$

$$f_{ck} = f_{cm} - \Delta f \tag{3.4.1.3}$$

where, f_{ck} is the characteristics compressive strength, f_{ctm} is the mean value of tensile strength and Δf is 8 MPa. The values used in this project were 2.18 MPa, 2.89 MPa and 3.52 MPa for low strength, medium strength and high strength concrete respectively.

- Uniaxial compression strength (FC) was taken as 33.7 MPa, 43.8 MPa and 55.2 MPa in this project in accordance with the experiment by Xiao and Wu (2000).

- Hardening parameter (HP) was taken as 0.01 as recommended in *Grassl et al (2013)* for all applications without strain rate.

- Tensile damage type (TYPE) was taken as 1, bi-linear damage formulation, as the bi-linear formulation is recommended by Grassl *et al* (2013) to obtain the best results.

- Tensile threshold value for linear tensile damage formulation (WF) was calculated, as recommended for TYPE 1 bi-linear softening, by using the equation:

$$WF = \frac{GF}{FT} \tag{3.4.1.4}$$

where, GF is the total fracture energy. Again, the required total fracture energy GF was calculated according to CEB-FIP Model Code (2010),

$$GF = 73.{f_{cm}}^{0.18} \tag{3.4.1.5}$$

where, f_{cm} is the compressive strength of concrete.

- Parameter controlling compressive damage softening branch in the exponential compressive damage formulation (EFC) was taken as 0.5 x 10^{-4}, which is a smaller value than the default one, as a smaller value provides more brittle form of damage.

The default values were used for other input variables. The detailed description of the input variables of MAT_CDPM is presented in Grassl (2016).

3.4.2 Material model for FRP Jacket

The material model used for FRP jacket was the '*MAT_ELASTIC or MAT_001'. This material model generally used for beam, shell and solid elements in LS-DYNA. There are 7 input variables in the elastic material model (*MAT_ELASTIC) card used in LS-DYNA (LSTC, 2017). Only 3 variables were needed to be determined for FRP jacket. They were mass density (RHO), Young's modulus (E), and Poisson's ratio (PR). Mass density and Poisson's ration were taken as 1000 kg/m^3 and 0.3 respectively for FRP jacket throughout this project. A value of 105 GPa was used for Young's modulus of FRP according to the data from experiment by Xiao and Wu (2000).

3.5 FE Analysis

The displacement control was used to analyze the finite element model to predict the response of FRP confined concrete. A mesh convergence study was performed for plain concrete model in order to determine the optimal mesh size that could provide accurate solution with reasonably short analysis time. The element mesh size of 0.03m, 0.04m, 0.05m and 0.07 m were used in the mesh convergence study with number of solid elements ranging from 139 to 2330. The finite element model for plain concrete with the mesh size of 0.03m, 0.04m, 0.05m and 0.07m is shown in figure 3.5.1.

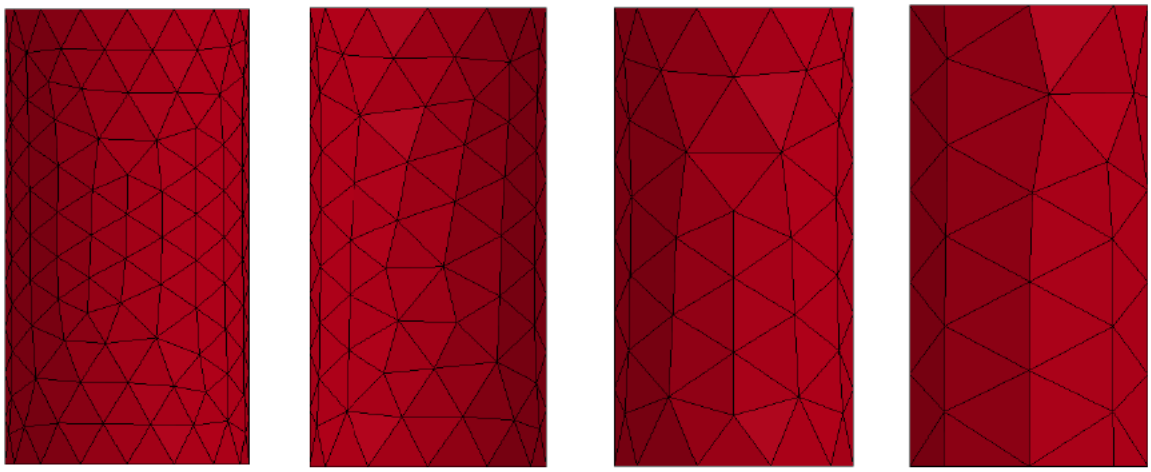

(a) (b) (c) (d)

Figure 3.5.1: Finite Element Mesh for Plain Conrete Model for (a) mesh size = 0.03m, (b) mesh size = 0.04m, (c) mesh size = 0.05m, and (d) mesh size = 0.07m

The best result was obtained from the mesh size of 0.05m. The FRP confined concrete was then modelled using the mesh size 0.05m. In FRP confined concrete model, there were 650 tetrahedron solid element for concrete core and 130 truss elements for FRP jackets. The final model is shown in figure 3.5.2.

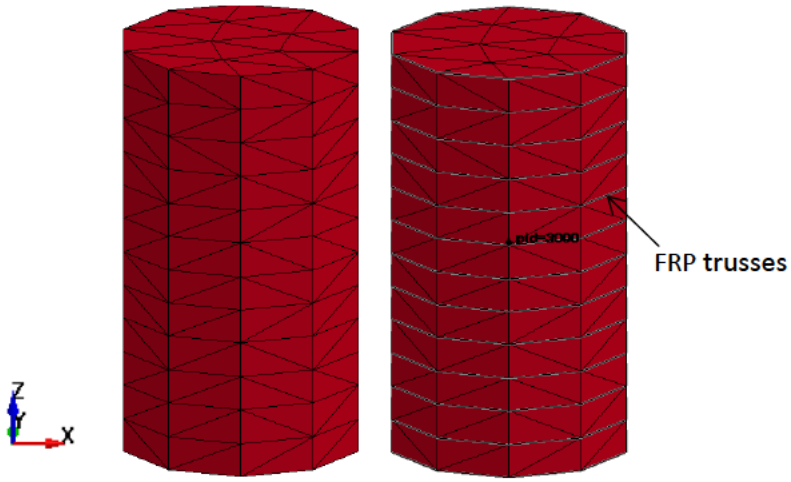

Figure 3.5.2: Final Model with Mesh Size of 0.05m

A total of 12 analyses were perfomed in this porject according to the experiment by Xiao and Wu (2000).

4. Results and Discussion

4.1 Comparison with Experiment Data and Proposed Model

Verification of FE model for the FRP confined concrete was done by comparing the results obtained from the FE modelling, using CDPM2, with the results obtained from the experiment performed by Xiao and Wu (2000). The experiment was explained in section 2.4.

The axial stress and axial strain curves and the axial stress and transverse strain curves were compared for low strength, medium strength and high strength concrete confined with FRP 0 layer, 1 layer, 2 layers and 3 layers.The positive axial strain values represent compressive strains and the negative transverse strain values represent tensile strains in the following section. The error % was calculated as:

$$Error\ (\%) = \frac{Exp\ result - FE\ model\ result}{Exp\ result} \times 100 \qquad (4.1.1)$$

and the % difference was calculated as:

$$\%\ Difference = \frac{Higher\ Value - FE\ model\ result}{Higher\ Value} \times 100 \qquad (4.1.1)$$

4.1.1 Low Strength:

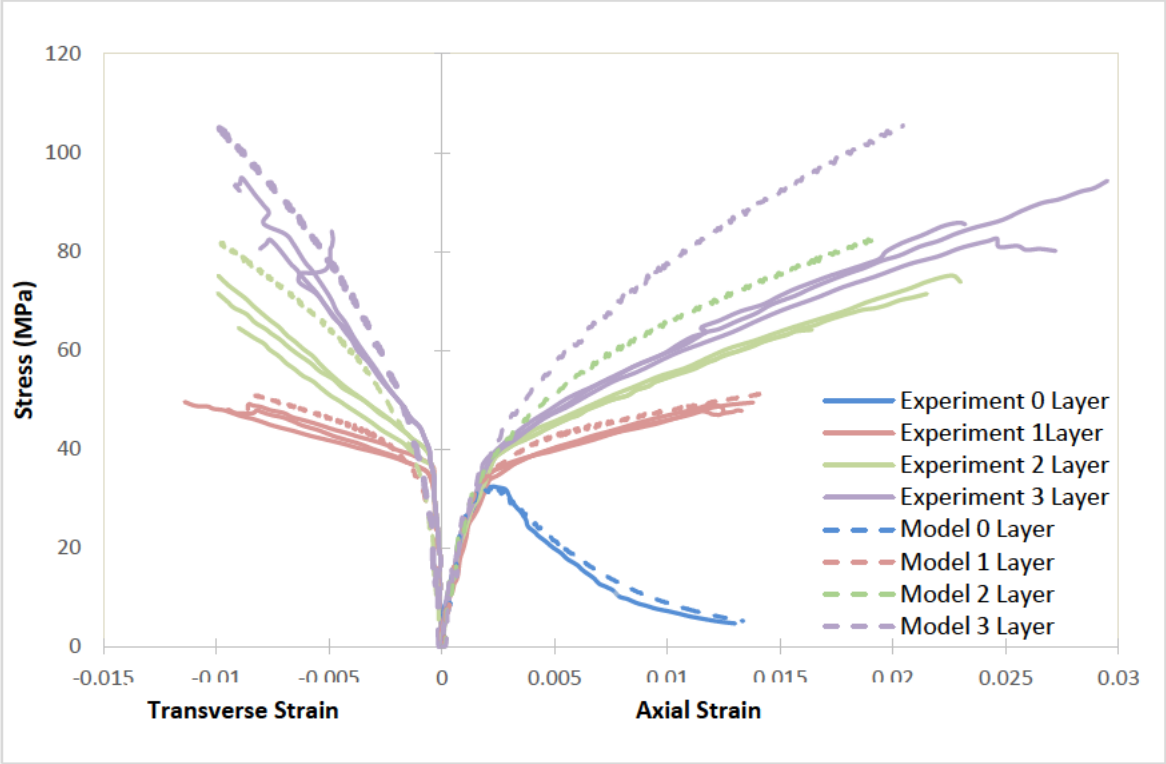

Figure 4.1.1.1: Stress VS Strain Relationship for CFRP Confined Concrete (Low Strength)

Figure 4.1.1.1 shows the experimental results versus the proposed model predictions for low strength concrete confined with FRPs. The predictions of the response for FRP 0 layer and 1 layer seems to be reasonable. The model could predict the maximum axial stress quite well for FRP 0-layer. The maximum axial stresses were 32.09MPa at axial strain of 0.002 for 32.3 MPa at axial strain of 0.00217 with an error of about 0.65%. For FRP confined models, the initial parts of the stress against axial strain curves are very well captured by the model. However, the model could not able to capture the response of the transition zone in stress versus transverse strain curves, where FRP jackets fully activates. In addition, the model overestimates the response of the ultimate confined stress. For stress versus axial strain curves, the error % are around -3.12%, -15.9% and -24% for FRP 1 layer, 2 layers and 3layers respectively. And for stress versus transverse strain curve, the error % are about -4.77%, -16.23% and -5.56% for FRP 1 layer, 2 layers and 3 layers respectively.

Therefore, it can be said that the volumetric expansion is overestimated and the error % increases with the FRP layers for low strength confined concrete model.

4.1.2 Medium Strngth:

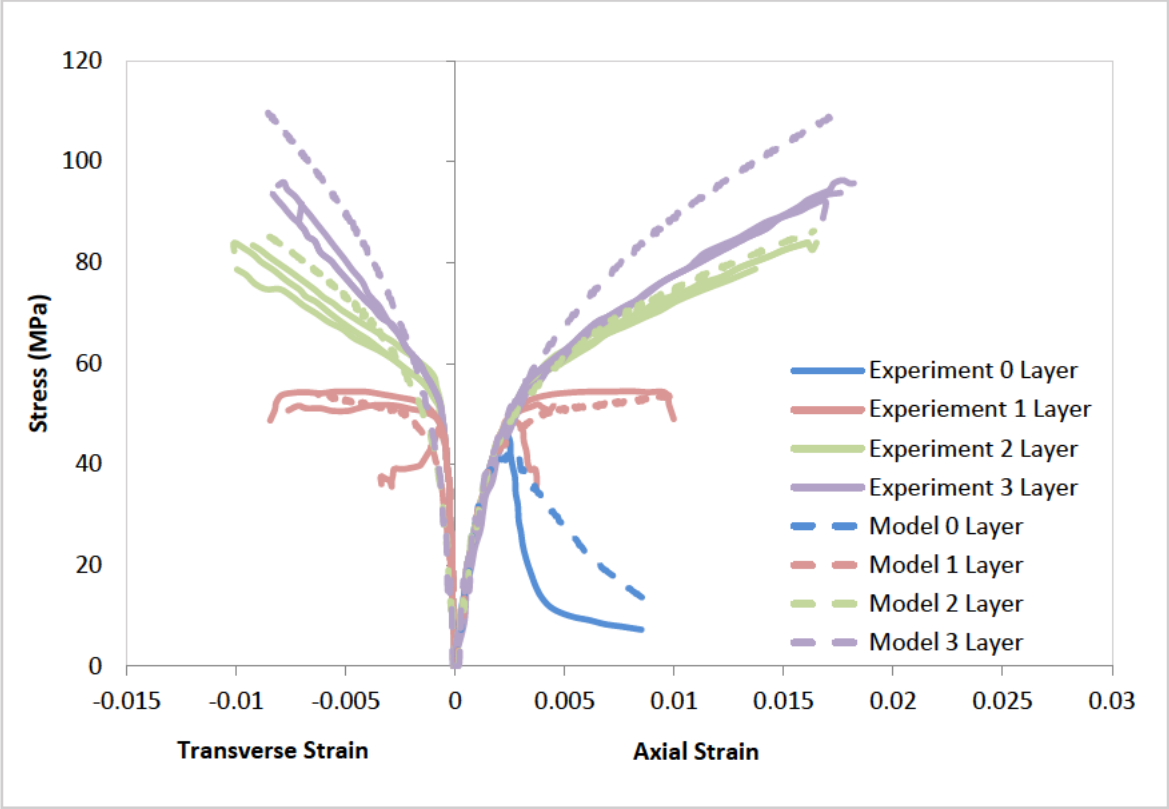

Figure 4.1.2.1: Stress VS Strain Relationship for CFRP Confined Concrete (Medium Strength)

Figure 4.1.2.1 shows the experimental results versus the proposed model predictions for medium strength concrete confined with FRPs. For FRP 0layer, there is a good agreement in the pre-peak response of stress-strain curve between the experimental results and the model predictions; however, the curve shows a significant difference at peak and post-peak regime. The model is not able to capture the strength reduction in the softening well. The maximum strength of concrete from experimental result is 45.3 MPa at the axial strain of 0.022, whereas, that of the model prediction is 41.05 MPa at the axial strain of 0.00203 producing an error of around 9.38%. The model seems to be able to capture the initial response of stress and axial strain curve very well. In addition, the response of FRP 1 layer and 2 layers shows a good agreement with the experimental results. However, the model overestimates the ultimate confinement. The % error for the stress versus axial strain curve are approximately -9.18%, -1.67% and -12.67 for FRP 1 layer, 2 layers and 3 layers respectively. Again, the % error for the stress versus transverse strain curve are around -7.5%, -6.05% and -13.24% for FRP 1 layer, 2 layers and 3 layers respectively.

Therefore, it can be said that the model response with the experimental results seems to agree well for FRP confined concrete. However, the volumetric expansion is overestimated for overestimated for FRP 2 layers and 3 layers.

4.1.3 High Strength:

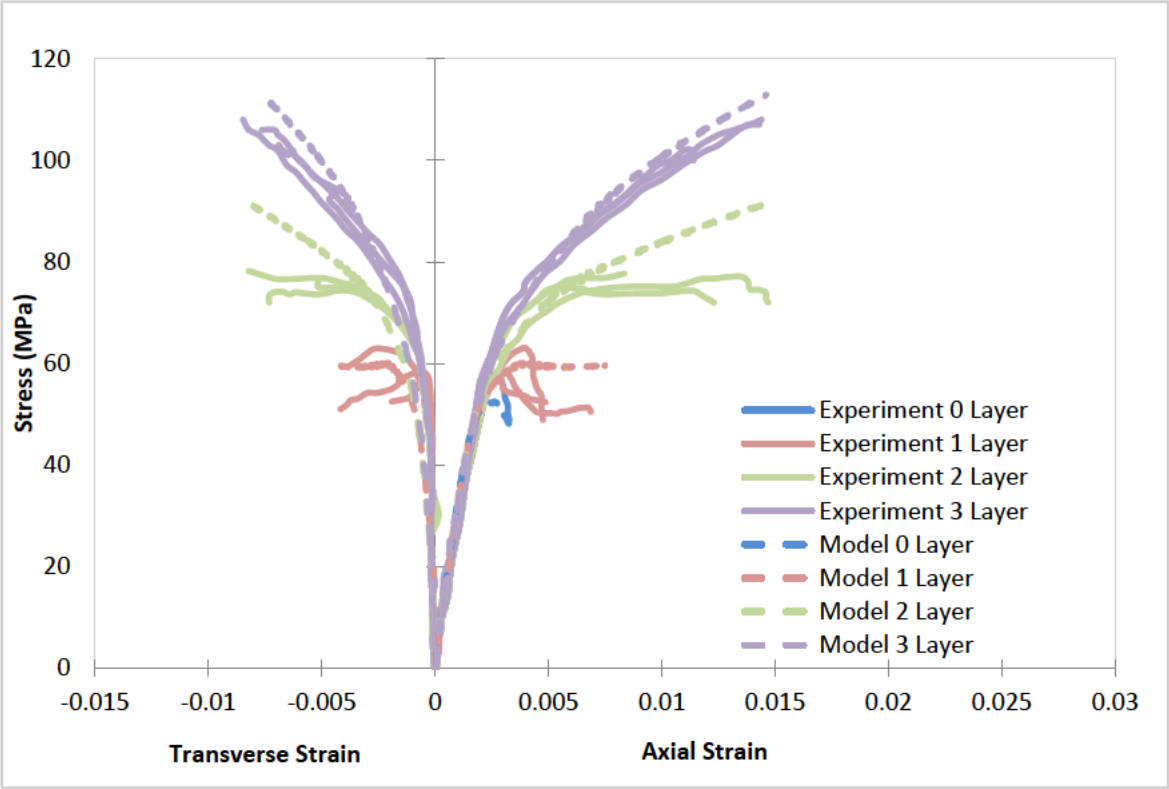

Figure 4.1.3.1: Stress VS Strain Relationship for CFRP Confined Concrete (High Strength)

Figure 4.1.3.1 shows the experimental results versus the proposed model predictions for high strength concrete confined with FRPs. The overall agreement of the model response with the experimental results seems to be very good, especially for FRP 1layer and 3layer. However, the model overestimates the ultimate confined strength. The error % for stress versus axial strain are around -6.76%, -21.88% and -3.52% for FRP 1 layer, 2 layers and 3 layers respectively, and the % error % for stress versus transverse strain are around -2.24%, 15.37% and -5.9%.

It can be said that the model agrees well with the experimental results for FRP 0 layer, 1 layer and 3 layers, but the model significantly overestimates the ultimate confined strength of FRP 2 layers.

4.1.4 Summary

In summary, although the model is not able to capture the stress strain response of the FRP confined concrete perfectly; the overall agreement of the experimental results with the model predictions seems to be good. The approximate error % of the model is presented in Table 4.1.3.1.

Table 4.1.4.1: Error % for the Experimental Results and Model Predictions

		Approximate Error % for Stress VS Axial Strain Curve	Approximate Error % for Stress VS Transverse Strain Curve
Low Strength Concrete	FRP 1 Layer	- 3.12%	-4.77%
	FRP 2 Layer	-15.9%	-16.23%
	FRP 3 Layer	-24%	-5.56%
Medium Strength Concrete	FRP 1 Layer	-9.18%	-7.5%
	FRP 2 Layer	-1.67%	-6.05%
	FRP 3 Layer	-7.5%	-13.24%
High Strength Concrete	FRP 1 Layer	-6.76%	-2.24%
	FRP 2 Layer	-21.88%	-15.37%
	FRP 3 Layer	-2.24%	-5.9%

4.2 Comparison with Analytical Model and Proposed Model

The axial stress-strain response of the FE model was validated with the response of the analytical model by Youssef *et al* (2007). The analytical model was explained in Section 2.6. In order to plot the stress-strain curve, confined modulus of elasticity E_c, axial stress f_t, axial strain ε_t, ultimate stress of FRP-confined concrete f'_{cu} and ultimate concrete compressive strain ε_{cu} were determined. Table 4.2.1 shows the results of analytical model.

Table 4.2.1: The Results of Analytical Model

Specimen	E_c	f_t	ε_t,	f'_{cu}	ε_{cu}
FRP 1 layer (Low Strength)	27284.30	36.86	0.0040	46.08	0.0108
FRP 2 layer (Low Strength)	27284.30	41.21	0.0052	63.14	0.0183
FRP 3 layer (Low Strength)	27284.30	46.17	0.0062	82.57	0.0257
FRP 1 layer (Medium Strength)	31105.34	46.56	0.0038	55.39	0.0091
FRP 2 layer (Medium Strength)	31105.34	50.83	0.0047	71.38	0.0148
FRP 3 layer (Medium Strength)	31105.34	55.48	0.0055	89.57	0.0206
FRP 1 layer (High Strength)	34919.45	57.99	0.0036	66.14	0.0075
FRP 2 layer (High Strength)	34919.45	61.84	0.0043	81.23	0.0125
FRP 3 layer (High Strength)	34919.45	66.22	0.0048	98.40	0.0015

Figure 4.2.1 shows the comparison of stress-strain curve of the confinement models for low strength, medium strength and high strength concrete. For low strength concrete; see fig 4.2.1a, the proposed model shows a good agreement with the analytical model for FRP 1-layer confined concrete. However, the proposed model predicts the ultimate confined strength significantly higher than the analytical model. In addition, the ultimate confined strength of FRP 2 layers predicted by the model is even higher than that of FRP 3 layer by the analytical model. The % difference are approximately 4.89% at the ultimate strain of 0.0108, 22.27% at the ultimate strain of 0.0183, and 29.32% at the ultimate strain of 0.0257 for FRP 1layer, 2 layers and 3layers confined concrete respectively.

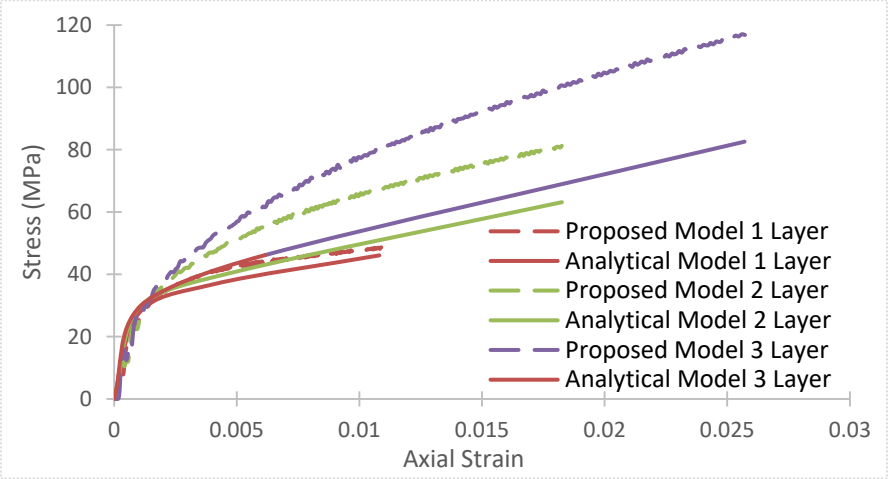

(a)

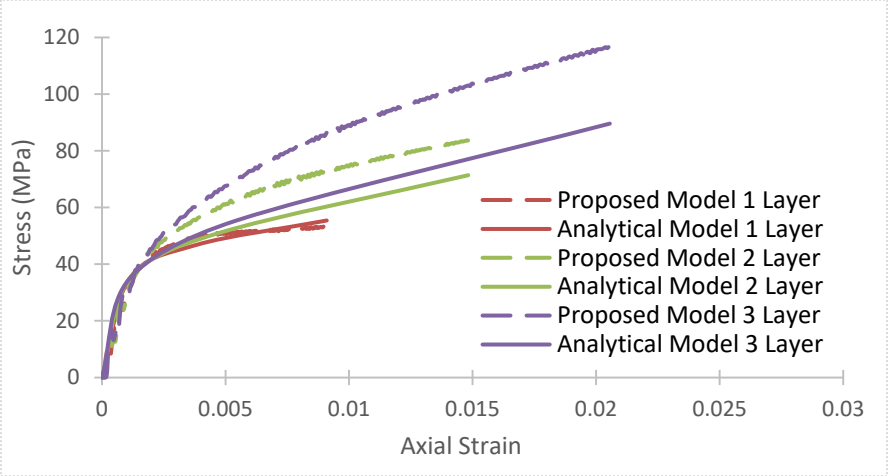

(b)

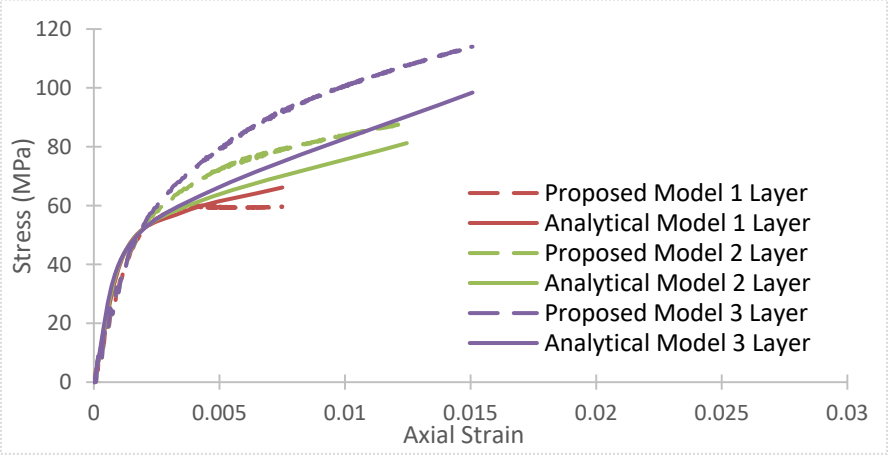

(c)

Figure 4.2.1: Comparison of Stress-Strain Curve of Confined Concrete Models for (a) Low Strength, (b) Medium Strength, and (c) High Strength

For medium strength concrete; see fig 8.2.1b, the overall agreement of the proposed model response with the analytical model response looks good. The proposed model predicts the ultimate confined strength slightly lower than the analytical model for FRP 1layer, whereas it overestimates the ultimate strength for FRP 2 layers and 3 layers. As in low strength, the model prediction for FRP 2 layers is even higher than FRP 3 layers predicted by the analytical model. The % difference are about 3.65% at the ultimate strain of 0.0091, 14.7% at the ultimate strain of 0.0125, and 23.33% at the ultimate strain of 0.0206 for FRP 1layer, 2 layers and 3 layers confined concrete respectively.

For high strength concrete; see fig 8.2.1c, a good agreement is obtained from the stress-strain response of the proposed model and the analytical model. As in medium strength, the proposed model seems to predict slightly lower value for the ultimate confined strength in FRP 1 layer than the analytical model. However, it predicts the ultimate confined strength higher than the analytical model. The % difference are around 9.78% at the ultimate strain of 0.0075, 7.69% at the ultimate strain of 0.0125, and 13.68% at the ultimate strain of 0.015 for FRP 1 layer, 2 layers and 3 layers confined concrete respectively.

Overall, the model seems to predict the ultimate confined strength quite well with the analytical model for FRP 1 layer in low strength and medium strength com, yet it predicts the higher values for FRP 2 layers and 3 layers in all low strength, medium strength and high strength. The % difference with the analytical prediction is between 3.65% to 29.32%.

4.3 Transverse Strain and Axial Strain Relationship

Figure 4.3.1 shows the relationship between the transverse strain versus axial strain for low strength, medium strength and high strength concrete confined with FRP 1layer, 2 layers and 3 layers. As can be from the figure, the graphs for FRP 1 layer, 2 layers and 3 layers shows the same trend all concrete strength, meaning that the level of lateral expansion of concrete decreases when the layer of FRP increases. This may be due to the fact that the lateral expansion is confined by the FRP jackets and the higher layers of FRP jackets produce the higher confining effect on the concrete.

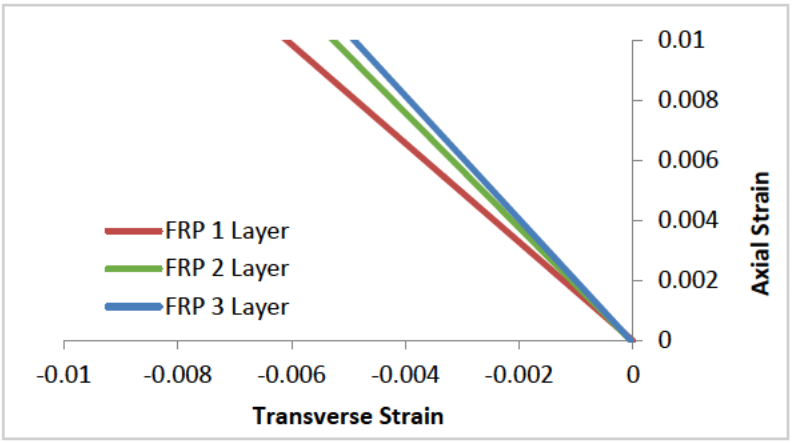

(a)

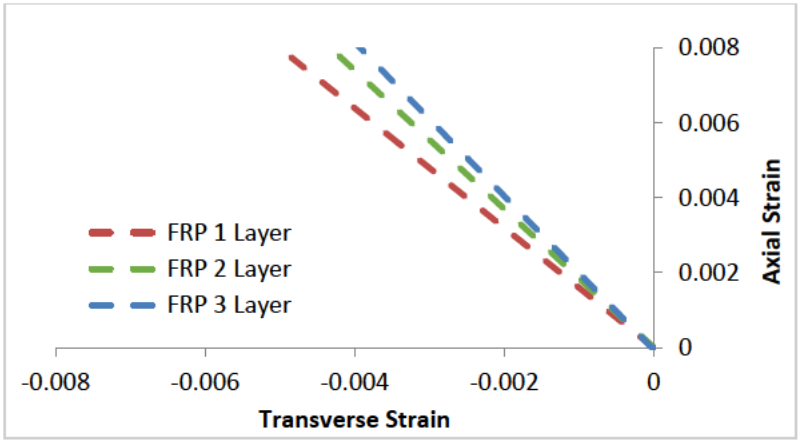

(b)

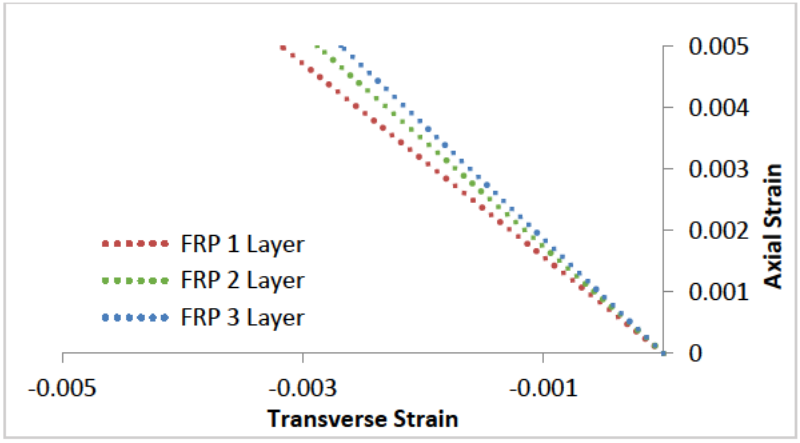

(c)

Figure 4.3.1: Transverse Strain VS Axial Strain for (a) Low Strength (b) Medium Strength, and (c) High Strength Concrete

Figure 4.3.2 shows the effect of concrete strength on FRP confinement the relationship between the transverse strain and axial strain. For all layers of FRP confinement, the lateral expansion increases with the strength of concrete. For FRP 1 layer, the variations between concrete strengths have very little effect on the lateral expansion. But for FRP 2 layers and 3 layers, the effect of lateral expansion seems to be more substantial with the variations between concrete strengths. It means the level of concrete strength might have the negative effect on the FRP confinement.

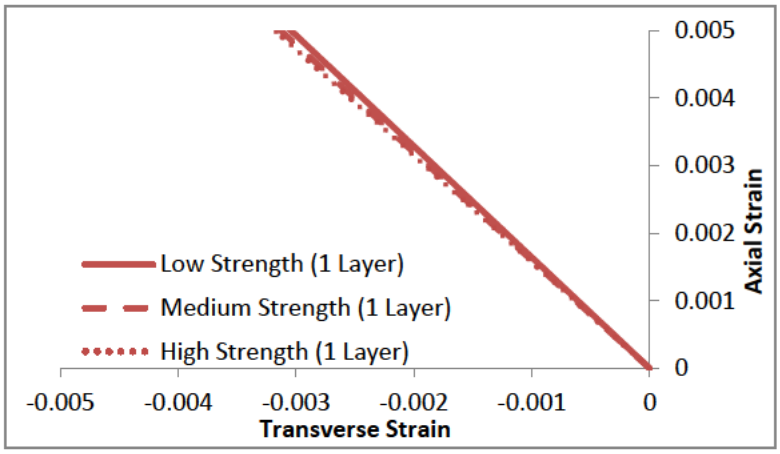

(a)

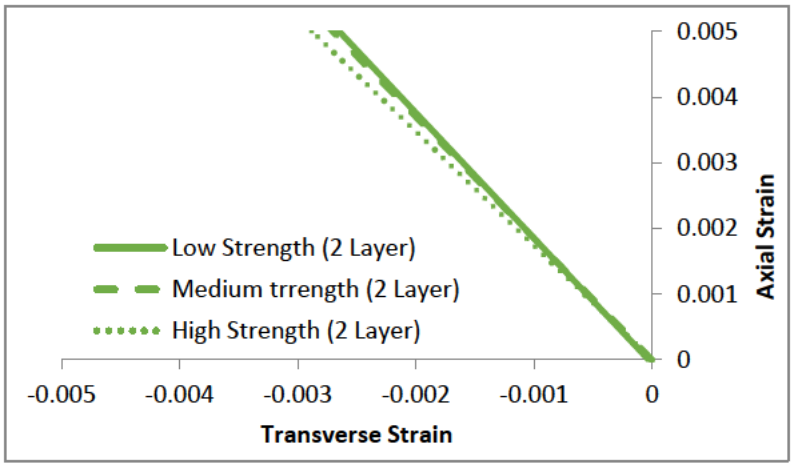

(b)

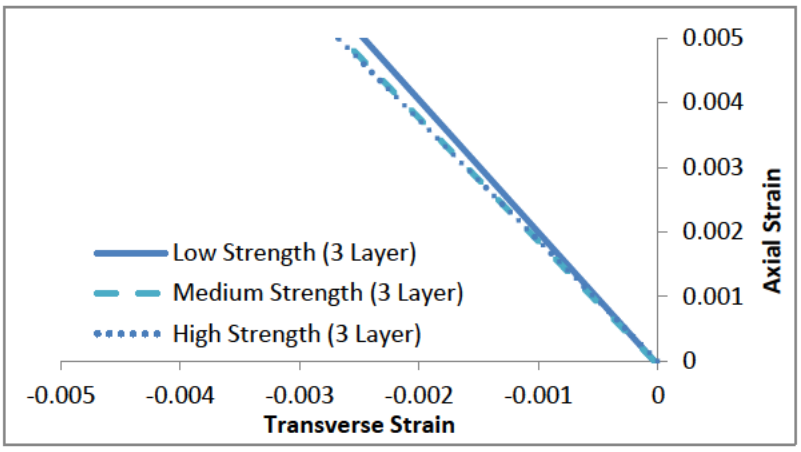

(c)

Figure 4.3.2: Transverse Strain VS Axial Strain for (a) FRP 1 Layer, (b) FRP 2 Layer, and (c) FRP 3 Layer Confined Concrete

4.4 Stress Variation in the Model

Stress variation in the model is analyzed for only high strength concrete. Figure 4.4.1 shows the contour plot for stress in axial direction at the same displacement.

The maximum stresses for all models occur at the top surfaces. This is because the compressive loading was applied on the top surface. In addition, the minimum stresses seem to appear at the corner of the top surfaces. This might be due to the the boundary conditions of the model: the nodes at the corner of the top surface were not constrained in X and Y direction.

As can be seen from the figure, the models with higher FRP layers create a plot with areas of greater stresses, meaning that the stiffness increases with the FRP layers.

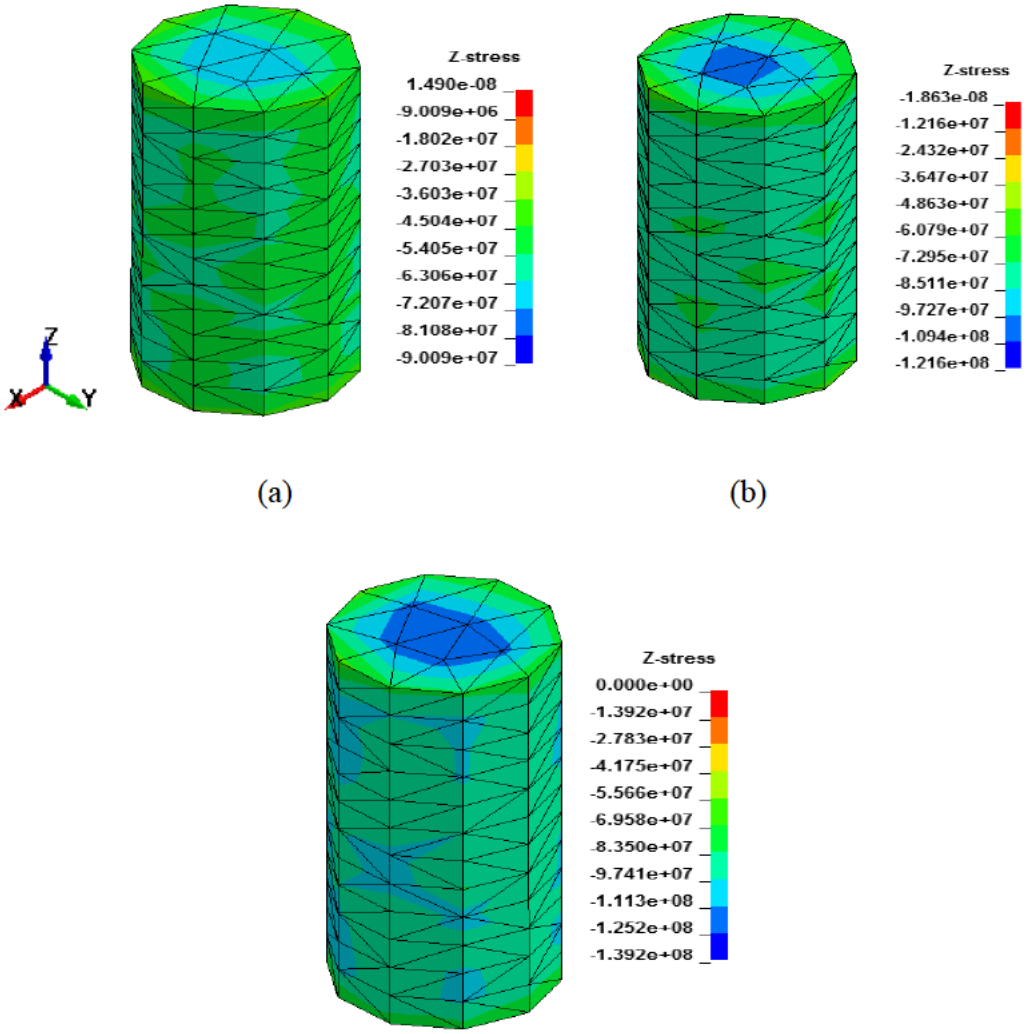

Figure 4.4.1: Z-Stress Contour Plot of High Strength Concrete with (a) FRP 1 Layer, (b) FRP 2 Layers, (c) 3 Layers

5. Conclusion and Further Research

5.1 Conclusion

This project is concerned with the development of FE model to predict the stress-strain relationship of FRP confined circular column with varying FRP layers and concrete strength. A number of factors were considered before modelling. These factors include the constituent materials model, complexity of the model, understanding of the software used, and advanced meshing method for nonlinear analysis of the structure. A total of 12 analyses are performed under uniaxial compression with displacement control in LS-DYNA. The model was validated against the experimental results and the analytical model results. The main conclusions of this project are summarized as follows:

- When comparing with the experimental results, the proposed model is able to predict the response of stress-strain curve of FRP 1 layer confined concrete quite well for all concrete strength. However, for FRP 2 layers and 3 layers, the volumetric expansion is overestimated. In addition, the model could not able to capture the response of the transition zone very well in stress versus transverse strain curves, where FRP jackets fully activates. The error % were approximately between -2.24% to -9.18% for FRP 1 layer, -1.67% to 21.88% for FRP 2 layers and -5.56% to -24% for FRP 3 layers. The average error % increases with the number of FRP layers.
- When comparing with the results from the analytical model, the overall agreement of the response of stress strain curve is quite well for FRP 1 layer in low and medium strength concrete. However, the ultimate confined stress is overestimated for FRP 2 layers and 3 layers in all concrete strength. The % difference with the analytical prediction is between 3.65% to 29.32%.
- The level of lateral expansion of concrete of the proposed model decreases when the layers of FRP increase. In addition, the level of concrete strength has the negative effect on the FRP confinement in the proposed model.
- The proposed model with higher FRP layers creates a plot with areas of greater stresses, meaning that the stiffness increases with the FRP layers.
- Overall, a fair correlation is achieved in predicting the actual performance of the cylinder columns with FRP jackets. However, the effect of FRP layer and concrete

strength is needed to be considered as the higher the FRP layers, the higher the % error.

5.2 Future Research

The effect of the number of FRP layers with the concrete strength is required to investigate for FE modelling. In addition, this project focused on concrete specimen under uniaxial compressive loading only. Therefore, future work should be focused on specimens under combined axial and seismic loading.

References

Benzarti, K. & Colin, X. (2013). Advanced Fibre-Reinforced Polymer (FRP) Composites for Structural Applications: Understanding the Durability of Advanced Fibre-Reinforced Polymer (FRP) Composites for Structural Applications. UK, Cambridge: Woodhead Publishing Limited.

Bhandari, D., & Thapa, K. B. (2014). Constitutive modelling of FRP Confined Concrete from Damage Mechanics. Saarbrücken, Germany: LAP LAMMBERT Academic Publishing.

Bright, N. and Roberts, J. (2010) "Structural Eurocodes: Extracts from the Structural Eurocodes for Students of Structural Design", 3rd Edition, London: BSI.

CEB-FIP Model Code (2010). Fib model code for concrete structures 2010. Document Competence Center Siegmar Kästl eK, Germany.

Daniel Rypl (2004). T3D Mesh Generator.Retrieved from: http://ksm.fsv.cvut.cz/~dr/t3d.html.

Desprez, C., Mazars, J., & Paultre, P. (2013). Damage model for FRP confined concrete columns under cyclic loading. Engineering Structures, 48, 519-531.

Fardis, M. N. & Khalili, H. H. (1982). FRP-encased Concrete as a Structural Material. Magazine of Concrete Research, 34(121), 191-201.

Giinaslan, S. E., Kaeasin, A. K., & Oncii, M. E. (2014). Properties of FRP Materials for Strengthening. International Journal of Innovative Science, Engineering & Technology, 1(9), 656-660.

Gowayed, Y. (2013). Types of fiber and fiber arrangement in fibre-reinforced polymer (FRP) composites. USA: Woodhead Publishing Limited.

Grassl, P., Xenos, D., Nyström, U., Rempling, R., & Gylltoft, K. (2013). CDPM2: A damage-plasticity approach to modelling the failure of concrete. International Journal of Solids and Structures, 50(24), 3805-3816.

Grassl, P., & Jirásek, M. (2006). Damage-plastic model for concrete failure. International journal of solids and structures, 43(22), 7166-7196.

Grassl, P. (2016). User Manual for MAT CDPM (MAT 273) in LS-DYNA. Retrieved from: http://petergrassl.com/Research/DamagePlasticity/CDPMLSDYNA/index.html#Manual

Habib, T. (2017). Properties of FRP Composites. Retrieved from https://www.academia.edu/23595537/Strengthening_rcc_column_using_FRP_composits.

Hearle, J.W.S. (Ed.) (2001), High Performance Fibers. Boca Raton: CRC Press.

Hollaway, L. (Ed.) (1990). Polymers and Polymer Composites in Construction. London: Thomas Telford Ltd.

Hu, D., & Barbato, M. (2014). Simple and efficient finite element modeling of reinforced concrete columns confined with fiber-reinforced polymers. Engineering Structures, 72, 113-122.

LSTC (2011). Livermore Software Technology Corporation. Retrieved from: http://www.lstc.com/products/ls-dyna.

LSTC (2017). LS-DYNA Keyword User's Manual Volume I, California: Livermore Software Technology Corporation.

LSTC (2017). LS-DYNA Keyword User's Manual Volume II Material Models, California: Livermore Software Technology Corporation.

LSTC (2017). LS-DYNA Theory Manual, California: Livermore Software Technology Corporation.

Murali, G. and Pannirselvam, N. (2011). Flexural Strengthening Of Reinforced Concrete Beams Using Fibre Reinforced Polymer Laminate: A Review. ARPN Journal of Engineering and Applied Sciences, 6 (11), 41-47.

Pan, Y., Li, H., Tang, H., & Huang, J. (2017). Analysis-oriented stress-strain model for FRP-confined concrtee with poreload. Composite Structures, 166, 57-67.

Piggott, M. (2004). Load Earing Fiber Composites, 2nd Edition. Boston/ Dordrecht/ London: Kluwer Academic Publishers.

Ramamoorthy, K., & Tamilamuthan, B. (2015). Modeling of High Strength Concrete Columns Confined with GFRP Wraps. Interantional Journal of Research in Engineering Science and Technologies, 1(7), 28-40.

Rashidi, M. (2014). Finite Element Modeling of FRP Wrapped High Strength Concrete Reinforced with Axial and Helical Reinforcement. International Journal of Emerging Technology and Advanced Engineering, 4(9), 728-735.

Shao, Y. (2003). Behavior of FRP-Concrete Beam-Column Under Cyclic Loading. Ralrigh: Retrieved from https://repository.lib.ncsu.edu/handle/1840.16/5788.

Singh, S. B. (2015). Analysis and Design of FRP Reinforced Concrete Structures. McGraw Hill Professional.

Xiao, Y., & Wu, H. (2000). Compressive Behavior of Concrete Confined by Carbon Fiber. Journal of Materials In Civil Engineering, 12(2), 139-146.

Youssef, M. N., Feng, M. Q., & Mosallam, A. S. (2007). Stress–strain model for concrete confined by FRP composites. Composites Part B: Engineering, 38(5), 614-628.

Youssf, O., ElGawady, M. A., Mills, J. E., & Ma, X. (2014). Finite element modelling and dilation of FRP-confined concrete columns. Engineering Structures, 79, 70-85.

Appendices

The following input files for low strength concrete confined with FRP 1 layer is taken as a sample input files. For other analyses, only area of FRP truss and variables concerned with concrete strength are changed.

Appendix 1 – Typical 'input.k' file

```
*KEYWORD
*TITLE
 Simulation of Single Small Brick subjected to tension
$
*Parameter
$---+----1----+----2----+----3----+----4----+----5----+----6----+----7----+----8
r Tstart    0.0     r Tend     1.e-2      r DtMax   100.e-3 r MaxDisp   -5.e-3
r TSSFAC    0.8     i LCTM      9         r TconP     30.0
$---+----1----+----2----+----3----+----4----+----5----+----6----+----7----+----8
$
*Parameter_Expression
$
 r TDplot    Tend/20
 r TASCII    TDplot/100.0
$
r Tend2    2.0*Tend
$
$
$   SOLID ELEMENT TIME HISTORY BLOCKS
*DATABASE_HISTORY_SOLID
$#     id1      id2      id3      id4      id5      id6      id7      id8
      563      680      716        0        0        0        0        0
$
*PART
$                                             title
concrete
$---+----1----+----2----+----3----+----4----+----5----+----6----+----7----+----8
$     pid     secid       mid     eosid      hgid      grav    adpopt      tmid
        1         1         1
```

```
$
*PART
$                                                  title
FRP truss
$---+----1----+----2----+----3----+----4----+----5----+----6----+----7----+----8
$     pid    secid     mid    eosid     hgid     grav   adpopt     tmid
     2000        2        2
$
*PART
$                                                  title
FRP truss boundary
$---+----1----+----2----+----3----+----4----+----5----+----6----+----7----+----8
$     pid    secid     mid    eosid     hgid     grav   adpopt     tmid
     3000        3        2
$
$
$
$---+----1----+----2----+----3----+----4----+----5----+----6----+----7----+----8
$
$
$
$$$$$$$$$$$$$$$$$$$$$$$$$$$$$$$$$$$$$$$$$$$$$$$$$$$$$$$$$$$$$$$$$$$$$$$$$$$$$$$$
$                          CONTROL OPTIONS                              $
$$$$$$$$$$$$$$$$$$$$$$$$$$$$$$$$$$$$$$$$$$$$$$$$$$$$$$$$$$$$$$$$$$$$$$$$$$$$$$$$
$
*CONTROL_ENERGY
       2        2        2        2
$---+----1----+----2----+----3----+----4----+----5----+----6----+----7----+----8
*CONTROL_SHELL
  20.0          1       -1        1        2        2        1
$---+----1----+----2----+----3----+----4----+----5----+----6----+----7----+----8
*CONTROL_TIMESTEP
$  DTINIT   TSSFAC     ISDO   TSLIMT    DT2MS     LCTM    ERODE    MS1ST
   0.0000      0.8        0    0.000    0.000    &LCTM
$---+----1----+----2----+----3----+----4----+----5----+----6----+----7----+----8
$
*CONTROL_TERMINATION
```

```
  &Tend
$
$
*CONTROL_OUTPUT
$  NPOPT NEECHO NREFUP IACCOP OPIFS IPNINT IKEDIT IFLUSH
    1,  3,    ,    ,   ,  50
$
$
$---+----1----+----2----+----3----+----4----+----5----+----6----+----7----+----8
$$$$$$$$$$$$$$$$$$$$$$$$$$$$$$$$$$$$$$$$$$$$$$$$$$$$$$$$$$$$$$$$$$$$$$$$$$$$$$$$
$                        TIME HISTORY                        $
$$$$$$$$$$$$$$$$$$$$$$$$$$$$$$$$$$$$$$$$$$$$$$$$$$$$$$$$$$$$$$$$$$$$$$$$$$$$$$$$
$
*DATABASE_ELOUT
$---+----1----+----2----+----3----+----4----+----5----+----6----+----7----+----8
$     dt
  &TASCII
$
*DATABASE_GLSTAT
$     dt
  &TASCII
$
*DATABASE_MATSUM
$     dt
  &TASCII
$
*DATABASE_NODFOR
$     dt
  &TASCII
*DATABASE_SPCFORC
$#     dt
  &TASCII
$---+----1----+----2----+----3----+----4----+----5----+----6----+----7----+----8
*DATABASE_BINARY_D3PLOT
$     dt
  &TDplot
$
```

```
$
$---+----1----+----2----+----3----+----4----+----5----+----6----+----7----+----8
*DATABASE_EXTENT_BINARY
$   neiph    neips    maxint   strflg   sigflg   epsflg   rltflg   engflg
     5                   1       1       1
$  cmpflg   ieverp   beamip
           0
$
$---+----1----+----2----+----3----+----4----+----5----+----6----+----7----+----8
*DATABASE_HISTORY_BEAM_SET
$---+----1----+----2----+----3----+----4----+----5----+----6----+----7----+----8
$   setid
     1
$
*SECTION_SOLID
$#  secid    elform      aet
$---+----1----+----2----+----3----+----4----+----5----+----6----+----7----+----8
     1       10       0
$
$
*SECTION_BEAM_TITLE
Section reinforcement
$---+----1----+----2----+----3----+----4----+----5----+----6----+----7----+----8
$      |       |       |       |       |       |       |       |
$   secid    elform     shrf   qr/irid     cst    scoor      nsm
     2       3             2            0.0      0.0
$      |       |       |       |       |       |       |       |
$      A    RAMPT    STRESS
  9.68e-6
$
$
*SECTION_BEAM_TITLE
Section reinforcement
$---+----1----+----2----+----3----+----4----+----5----+----6----+----7----+----8
$      |       |       |       |       |       |       |       |
$   secid    elform     shrf   qr/irid     cst    scoor      nsm
     3       3             2            0.0      0.0
```

```
$      |       |       |       |       |       |       |       |
$      A    RAMPT    STRESS
  4.84e-6
$
$ Material
$
*Include
material.k
$
$---+----1----+----2----+----3----+----4----+----5----+----6----+----7----+----8
*Boundary_Prescribed_Motion_Set
$---+----1----+----2----+----3----+----4----+----5----+----6----+----7----+----8
$      ID      DOF      VAD      LCID      SF      VID    DEATH    BIRTH
       1       3       2      111      1.0
$
$ applied Y-direction displacement
*DEFINE_CURVE
 111, 0, 1., 1., 0., 0.
  0.0,    0.0
  &Tend,   &MaxDisp
  &Tend2,  &MaxDisp
$
$
$ maximum time increment
*DEFINE_CURVE
9,0,1.,1.,0.,0.
   0.0,  &DtMax
 &Tend,  &DtMax
 &Tend2, &DtMax
$$$$$$$$$$$$$$$$$$$$$$$$$$$$$$$$$$$$$$$$$$$$$$$$$$$$$$$$$$$$$$$$$$$$$$$$$$$$$$$$
$                       BOUNDARY DEFINITIONS                       $
$$$$$$$$$$$$$$$$$$$$$$$$$$$$$$$$$$$$$$$$$$$$$$$$$$$$$$$$$$$$$$$$$$$$$$$$$$$$$$$$
$
*Include
mesh.k
*END
```

Appendix 2 – Typical ‘mesh.k’ file

```
$ Material
$ Mat 273 (units: Newtons-m-Pa)
*MAT_CDPM
$---+----1----+----2----+----3----+----4----+----5----+----6----+----7----+----8
$      |       |       |       |       |       |       |       |
$     MID      RHO       E      PR     ECC     QH0      FT      FC
       1   2.30E3   30.16E9     0.2              2.18e6   33.7e6
$      |       |       |       |       |       |       |       |
$     HP      AH      BH      CH      DH      AS      DF     FC0
    0.01                              15
$      |       |       |       |       |       |       |       |
$    TYPE      BS      WF     WF1     FT1   STRFLG   FAILFLG     EFC
       1       1  270.3e-6                           0.5e-4
$
$
$
*MAT_ELASTIC
$---+----1----+----2----+----3----+----4----+----5----+----6----+----7----+----8
$      |       |       |       |       |       |       |       |
$#    mid      ro       e      pr      da      db  not used
       2    1.e3    105.E9    0.32
$
```

Appendix 3 – Typical ‘material.k’ file

```
$# LS-DYNA Keyword file created by LS-PrePost(R) V4.5.0 (Beta) - 06Jun2017
$# Created on Jul-20-2017 (09:01:51)
*KEYWORD
*TITLE
$#                                                 title
LS-DYNA keyword deck by LS-PrePost
*BOUNDARY_SPC_SET
$#   nsid     cid    dofx    dofy    dofz   dofrx   dofry   dofrz
     2       0       1       1       0       0       0       0
*SET_NODE_LIST_TITLE
NODESET(SPC) 2
$#    sid     da1     da2     da3     da4   solver
     2     0.0     0.0     0.0     0.0MECH
$#   nid1    nid2    nid3    nid4    nid5    nid6    nid7    nid8
    137       0       0       0       0       0       0       0
*BOUNDARY_SPC_SET
$#   nsid     cid    dofx    dofy    dofz   dofrx   dofry   dofrz
     3       0       0       0       1       0       0       0
*SET_NODE_LIST_TITLE
NODESET(SPC) 3
$#    sid     da1     da2     da3     da4   solver
     3     0.0     0.0     0.0     0.0MECH
$#   nid1    nid2    nid3    nid4    nid5    nid6    nid7    nid8
     1       2      27      28      29      30      31      32
    33      34     131     132     133     134     135       0
*BOUNDARY_SPC_SET
$#   nsid     cid    dofx    dofy    dofz   dofrx   dofry   dofrz
     4       0       1       1       0       0       0       0
*SET_NODE_LIST_TITLE
NODESET(SPC) 4
$#    sid     da1     da2     da3     da4   solver
     4     0.0     0.0     0.0     0.0MECH
$#   nid1    nid2    nid3    nid4    nid5    nid6    nid7    nid8
    132       0       0       0       0       0       0       0
*SET_BEAM
$#    sid
```

```
      1
$#     k1      k2      k3      k4      k5      k6      k7      k8
    2001    2002    2003    2004    2005    2006    2007    2008
    2009    2010    2011    2012    2013    2014    2015    2016
    2017    2018    2019    2020    2021    2022    2023    2024
    2025    2026    2027    2028    2029    2030    2031    2032
    2033    2034    2035    2036    2037    2038    2039    2040
    2041    2042    2043    2044    2045    2046    2047    2048
    2049    2050    2051    2052    2053    2054    2055    2056
    2057    2058    2059    2060    2061    2062    2063    2064
    2065    2066    2067    2068    2069    2070    2071    2072
    2073    2074    2075    2076    2077    2078    2079    2080
    2081    2082    2083    2084    2085    2086    2087    2088
    2089    2090    2091    2092    2093    2094    2095    2096
    2097    2098    2099    2100    2101    2102    2103    2104
    2105    2106    2107    2108    2109    2110    2111    2112
    2113    2114    2115    2116    2117    2118    2119    2120
    2121    2122    2123    2124    2125    2126    2127    2128
    2129    2130       0       0       0       0       0       0
*SET_NODE_LIST
$#    sid     da1     da2     da3     da4    solver
      1     0.0     0.0     0.0     0.0MECH
$#   nid1    nid2    nid3    nid4    nid5    nid6    nid7    nid8
      3       4      35      36      37      38      39      40
     41      42     136     137     138     139     140       0
*ELEMENT_SOLID
$#  eid    pid     n1     n2     n3     n4     n5     n6     n7     n8
   131      1      6      2     46    133    133    133    133    133
   132      1      8      6     46    141    141    141    141    141
   133      1     10      8     62    142    142    142    142    142
   133      1     10      8     62    142    142    142    142    142
   134      1     12     10     70    143    143    143    143    143
   135      1     14     12     70    143    143    143    143    143
   136      1     16     14     86    144    144    144    144    144
   137      1     18     16     94    145    145    145    145    145
   138      1     20     18     94    145    145    145    145    145
   139      1     22     20    110    146    146    146    146    146
```